


Tracking the delayed response of the northern winter stratosphere to ENSO using multi reanalyses and model simulations

Rongcai Ren^{1,2}  · Jian Rao^{1,2,3} · Guoxiong Wu¹ · Ming Cai⁴

Received: 22 February 2016 / Accepted: 12 June 2016 / Published online: 22 June 2016
© Springer-Verlag Berlin Heidelberg 2016

Abstract The concurrent effects of the El Niño-Southern Oscillation (ENSO) on the northern winter stratosphere have been widely recognized; however, the delayed effects of ENSO in the next winter after mature ENSO have yet to be confirmed in multi reanalyses and model simulations. This study uses three reanalysis datasets, a long-term fully coupled model simulation, and a high-top general circulation model to examine ENSO's delayed effects in the stratosphere. The warm-minus-cold composite analyses consistently showed that, except those quick-decaying quasi-biennial ENSO events that reverse signs during July–August–September (JAS) in their decay years, ENSO events particularly those quasi-quadrennial (QQ) that persist through JAS, always have a significant effect on the extratropical stratosphere in both the concurrent winter and the next winter following mature ENSO. During the concurrent winter, the QQ ENSO-induced Pacific-North American (PNA) pattern corresponds to an anomalous wavenumber-1 from the upper troposphere to the stratosphere, which acts to intensify/weaken the climatological wave pattern during warm/cold ENSO. Associated with

the zonally quasi-homogeneous tropical forcing in spring of the QQ ENSO decay years, there appear persistent and zonally quasi-homogeneous temperature anomalies in the mid-latitudes from the upper troposphere to the lower stratosphere until summer. With the reduction in ENSO forcing and the PNA responses in the following winter, an anomalous wavenumber-2 prevails in the extratropics. Although the anomalous wave flux divergence in the upper stratospheric layer is still dominated by wavenumber-1, it is mainly caused by wavenumber-2 in the lower stratosphere. However, the wavenumber-2 activity in the next winter is always underestimated in the model simulations, and wavenumber-1 activity dominates in both winters.

Keywords ENSO · Delayed effects · Northern winter stratosphere

1 Introduction

Existing evidence has demonstrated the concurrent effects of El Niño-Southern Oscillation (ENSO) in the extratropical stratosphere during mature ENSO winters; i.e., the northern winter stratospheric polar vortex is anomalously weak/strong in warm/cold ENSO winters (e.g., van Loon et al. 1982; Wallace and Chang 1982; Labitzke and van Loon 1989; Camp and Tung 2007; Garfinkel and Hartmann 2007, 2008), despite the possibly entangled signals of the quasi biennial oscillation (QBO) in the equatorial stratosphere (e.g., Wei et al. 2007; Garfinkel and Hartmann 2007, 2008; Calvo et al. 2009). The significant concurrent effects of ENSO in the stratosphere have also been verified in model simulations (Hamilton 1995; Sassi et al. 2004; Taguchi and Hartmann 2006; Manzini et al. 2006; García-Herrera et al. 2006; Rao et al. 2015; Rao and Ren 2016).

✉ Rongcai Ren
rrc@lasg.iap.ac.cn

¹ State Key Laboratory of Numerical Modeling for Atmospheric Sciences and Geophysical Fluid Dynamics, Institute of Atmospheric Physics, Chinese Academy of Sciences, 100029 Beijing, China

² Collaborative Innovation Center on Forecast and Evaluation of Meteorological Disasters, KLME, and College of Atmospheric Science, Nanjing University of Information Science and Technology, 210044 Nanjing, China

³ College of Earth Science, University of Chinese Academy of Sciences, 100049 Beijing, China

⁴ Department of Earth, Ocean, and Atmospheric Science, Florida State University, Tallahassee 32306, USA

A warm ENSO is to induce an anomalous Pacific-North American (PNA)-like pattern in the extratropical upper troposphere and mainly enhance the wavenumber-1 in the stratosphere, thus resulting in polar warming during the late winter or early spring of warm ENSO years (Taguchi and Hartmann 2006; Manzini et al. 2006).

Recent evidence has indicated the existence of a delayed effect of ENSO on the extratropical stratosphere. Manzini et al. (2006) noticed a time lag of the polar warming in the lower stratosphere relative to the upper stratosphere during warm ENSO years. García-Herrera et al. (2006) indicated that the maximum warming response in the polar stratosphere to warm ENSO forcing does not appear in the month of the maximum Niño 3.4 value, but lags by several months. In addition, Chen et al. (2003) showed that the maximum significant correlation between an ENSO index and the meridional Eliassen–Palm (E–P) flux divergence at 30 hPa exists when the ENSO peak leads that of the E–P flux by about three seasons. Ren et al. (2012) demonstrated that the polar stratosphere is anomalously warm/cold, not only in the concurrent winter, but also in the next winter after warm/cold ENSO when it is in a 3–5 years timescale. They also indicated that the warming/cooling responses in the extratropical stratosphere in the next winter may, on average, be even stronger, with a deeper vertical structure than that in the concurrent winter. They further emphasized that, in relation to the delayed effect of ENSO on the upper troposphere (Newell and Weare 1976; Angell 1981; Reid et al. 1989; Yulaeva and Wallace 1994; Kumar and Hoerling 2003), there exist persistent and zonally homogeneous warm anomalies in the midlatitude stratosphere during the summer of ENSO decay years, which are directly followed by stratospheric polar warming in the next winter after mature ENSO. Evtushevsky et al. (2015) also reported a possible delayed effect of the tropical central Pacific sea surface temperature (SST) forcing on the southern extratropical stratosphere.

However, variations in ENSO behavior are not restricted to the 3–5 year timescale. For example, some studies have indicated that ENSO has two dominant frequency bands: the 3–5 year quasi-quadrennial (QQ) cycle, and the quasi-biennial (QB) cycle (Jiang et al. 1995; Bejarano and Jin 2008). Other studies indicated that the dominant variations of ENSO include a QB mode and a low frequency (LF) mode that covers a time period of 3–7 years (Barnett 1991; Kim and Kim 2002; Wang and An 2005). In addition, a near-annual mode of ENSO was indicated (Jin et al. 2003; Tozuka and Yamagata 2003), and occasions of “follow-up” La Niña after La Niña were identified (Hu et al. 2014). By focusing on the various ENSO events of the past 60 years, preliminary investigations indicated that, when peaks in ENSO events appear beyond winter–spring seasons, ENSO’s effect on the extratropical stratosphere

may be confined to the concurrent winter of mature ENSO, rather than delayed until the next winter (Ren 2012a, b). Due to the limited length of the data record currently available, and the strong diversity of ENSO variations, the existence of the delayed effect of ENSO on the stratosphere and the responsible physical processes remain to be validated in more datasets and in model simulations. In particular, we must explore the circumstances under which the ENSO’s influences on the stratosphere are confined to the concurrent winter of a mature ENSO. Also, in which case can the influences of ENSO be extended or delayed until the next winter after mature ENSO? The answers to these questions require further clarifications.

This study uses three reanalysis datasets, together with the long-term CMIP5 (Coupled Model Intercomparison Project phase 5; Taylor et al. 2012) simulation records from the fully coupled earth system model (ESM) CESM-WACCM (Danabasoglu et al. 2012; Holland et al. 2012; Marsh et al. 2013) to examine the possible delayed effects of the different types of ENSO events on the extratropical stratosphere. We also use the “high top” Whole Atmosphere Community Climate Model (WACCM), which has been successfully used to investigate the stratospheric response to ENSO forcing (Sassi et al. 2004; Calvo et al. 2010; Rao and Ren 2016), and to perform a series of sensitivity experiments to further verify the existence of ENSO’s delayed effects on the extratropical stratosphere, as well as to clarify the related physical processes. The results will further advance our knowledge of the influence of ENSO on the stratosphere and improve our understanding of the interannual variability of the extratropical stratosphere.

The remainder of this paper is organized as follows. Section 2 introduces the reanalysis datasets, the simulation records from a fully coupled ESM, the atmospheric model WACCM, and the experiment design. Section 3 demonstrates the different spatio-temporal features of the various forms of ENSO in the reanalysis data and in the model simulations. In Sect. 4, we investigate the existence/non-existence of the delayed response of the stratosphere to the different types of ENSO. Section 5 provides modeling evidence of the delayed response of the stratosphere to ENSO, from both the coupled CMIP ESM simulations and the WACCM experiments. Finally, a discussion and summary are provided in Sect. 6.

2 Data, models, and experiment design

2.1 Reanalysis datasets

The three reanalysis datasets used in this study are the National Centers for Environmental Prediction–National Center for Atmospheric Research Reanalysis I (NCEP/

NCAR) covering the period 1958–2012 (Kalnay et al. 1996); the European Centre for Medium-Range Weather Forecast's Reanalysis (ERA) dataset, which was constructed by concatenating its 40-year Reanalysis (ERA40) covering the period 1958–2001 (Uppala et al. 2005) with its Interim Reanalysis (ERA-I; Dee et al. 2011) data record from 2002 to 2012; and the Japanese 55-year Reanalysis (JRA55) covering the period 1958–2012 (Ebita et al. 2011; Kobayashi et al. 2015). The NCEP/NCAR reanalysis was extracted from 1958 (the International Geophysical Year, IGY) to 2012 to avoid the data uncertainties before 1958 (Kalnay et al. 1996) and to keep the consistency with the timespan covered by the other two datasets. A spatial interpolation was performed on the ERA-I data fields to transform the horizontal resolution from $1.0^\circ \times 1.0^\circ$ to $2.5^\circ \times 2.5^\circ$ longitude–latitude grids before concatenation with ERA40. More detailed descriptions of the three reanalysis datasets can be found in the related references (Kalnay et al. 1996; Uppala et al. 2005; Dee et al. 2011; Ebita et al. 2011). The circulation anomaly fields were obtained by removing the annual cycle and a long-term trend from the monthly mean total fields. In addition, the Lanzos band-pass-filtering (Duchon 1979) with a cutoff period of 24–32 months was applied to the circulation anomaly fields in the stratosphere above 100 hPa, and then the QBO-related changes were subtracted from the original data before the composite analysis was performed, to prevent the possible entanglement of QBO signals.

After confirming the general consistent representation of ENSO events among the SST datasets, including the masked skin temperature from the NCEP/NCAR reanalysis, the Met Office Hadley Center's sea ice and sea surface temperature (HadISST) dataset (Rayner et al. 2003), and the Japan Meteorological Agency's centennial in situ observation-based estimates (COBE; Ishii et al. 2005), we used the monthly mean SST anomalies from the HadISST dataset to define the ENSO signals. After removing the long-term trend and the annual cycle of the SST fields, we calculated the monthly Niño3 index by averaging the SST anomalies over the Niño3 region (5°S – 5°N , 150 – 90°W). We defined ENSO events when the December–January–February (DJF) Niño3 index exceeded its unit standard deviation (0.82°C).

To demonstrate the possibly different effects of ENSO on the stratosphere, we categorized the ENSO events based on their different seasonal variations. That is, an ENSO event was classified as a quasi-quadrennial (QQ) ENSO when its polarity remained un-reversed throughout the following summer, with the signs of the Niño3 index persisting from DJF to the following July–August–September (JAS). Alternatively, the ENSO event was classified as a quasi-biennial (QB) ENSO when its polarity was reversed before JAS. The identified QQ and QB El Niño and La

Niña events from the HadISST dataset are listed in Table 1. It should be noted that the QQ/QB ENSO events, as defined here, may not denote only those events that restrictedly followed a quasi-quadrennial/quasi-biennial timescale, as was the case in previous studies (Jiang et al. 1995; Bejarano and Jin 2008). However, as will be seen from Fig. 1 in Sect. 3, the QQ/QB ENSO events, on average, do show a generally quasi-quadrennial/quasi-biennial periodicity, implying that the majority of these events did follow a quasi-quadrennial or quasi-biennial timescale, respectively. Next, we will show that the existence of the delayed effects of ENSO on the stratosphere is indeed tied to the contrasting seasonal variations of the Niño3 index between these QQ and QB types.

2.2 CESM-WACCM and its CMIP5 simulation dataset

Compared with the Community Climate System Model version 4 (CCSM4; Gent et al. 2011), the atmospheric components of CESM version 1 (CESM1) include a “high top” version, the WACCM (version 4) that incorporates fully interactive chemistry and has 66 vertical levels up to 5.1×10^{-6} hPa (approximately 140 km) with a horizontal resolution of 1.9° (latitude) \times 2.5° (longitude). WACCM has been used to study long-term changes caused by increasing levels of greenhouse gases (Garcia et al. 2007), the development and recovery of the ozone hole (Eyring et al. 2007, 2010a, b), and the atmospheric response to the solar cycle and the flux of energetic particles (e.g., Marsh et al. 2007; Jackman et al. 2009; Matthes et al. 2010). In particular, it has been used to investigate the atmospheric response of the stratosphere to tropical ENSO forcing (Sassi et al. 2004; Calvo et al. 2010; Rao and Ren 2016). In essence, version 4 of WACCM (WACCM4) is a superset of the Community Atmospheric Model version 4 (CAM4) and includes all of the physical parameterizations in CAM4 (Neale et al. 2013). Notable improvements in WACCM4 include parameterization of non-orographic gravity waves generated by frontal systems and convection, and particularly the parameterization of the surface stress by unresolved topography (Garcia et al. 2007; Richter et al. 2010), which has led to a dramatic improvement in the simulation of the frequency of northern winter stratospheric sudden warming events (Richter et al. 2010; Marsh et al. 2013). QBO signals in WACCM4 can optionally be imported by relaxing the equatorial zonal wind between 86 and 4 hPa to the observed (Matthes et al. 2010). For the CMIP5 simulations, CESM-WACCM uses active ocean and sea ice components as described by Holland et al. (2012) and Danabasoglu et al. (2012).

The CMIP5 simulations (<http://cmip-pcmdi.llnl.gov/cmip5/availability.html>) from CESM-WACCM are listed in Table 2. In addition to a 200-year “piControl” simulation

Table 1 List of ENSO events over the period 1958–2012 in observation

ENSO type	Years	Average D ⁰ J ¹ F ¹ Niño3 (K)	Events duration (Start Time–End time)
El Niño	QQ 1957/58, 1965/66, 1968/69, 1976/77, 1986/87, 1991/92, 2002/03	1.07	March 1957–Sept 1958, March 1963–March 1964, April 1965–July 1966, June 1968–March 1970, March 1972–March 1973, May 1976–Feb 1978, Aug 1982–July 1983, Aug 1986–March 1988, March 1991–Aug 1992, Aug 1994–April 1995, March 1997–June 1998, March 2002–March 2004, June 2006–Feb 2007, April 2009–May 2010
	QB 1963/64, 1969/70, 1972/73, 1982/83, 1987/88, 1994/95, 1997/98, 2006/07, 2009/10	1.59	
La Niña	QQ 1970/71, 1973/74, 1984/85, 1988/89, 1995/96, 1998/99	–1.12	Jan 1962–March 1963, Feb 1964–March 1965, March 1970–Feb 1972, March 1973–Aug 1974, March 1975–April 1976, Sept 1983–July 1986, Feb 1988–Jan 1990, Apr 1995–April 1997, June 1998–April 2000, April 2001–March 2002, July 2005–June 2006
	QB 1962/63, 1964/65, 1971/72, 1975/76, 1996/97, 2001/02, 2005/06	–0.82	

with all external forcings fixed at 1850 values, there are seven runs that were forced with observed forcings: one from 1850 to 2005 (Historical-R1) and the other six runs from 1955 to 2005 but with different initial conditions (R2–R7). The forcings include the changes in the surface concentration of active radiative species, daily solar spectral irradiance, and volcanic sulfate heating.

To greatly increase the number of ENSO events that could be identified from the fully coupled simulations, we used the results from all of these experiments. Specifically, we first derived the SST and atmospheric circulation anomalies by removing the corresponding climatology from the original fields separately for each ensemble run, and then removed a linear trend and the possible stratospheric QBO signals from the anomaly fields (as for the reanalysis data). Finally, we concatenated the anomaly data from all experiments along the time dimension and generated a long time series covering more than 7000 months. We deliberately added a conjunct node between any two adjacent datasets and set it to be unfilled to avoid any identification of ENSO events across datasets (two manuscripts by Rao and Ren revised to *Journal of Geophysical Research*). The criterion we used to identify ENSO events from the model time series was roughly the average unit standard deviation of the Niño3 index for all experiments (ca. 1.13 K). Similarly, the ENSO events in these simulations were categorized as either QQ or QB types as for the reanalysis data. The total numbers of QQ and QB events, as well as the composite ENSO amplitudes, are listed in Table 3. By referring to Table 1, it is seen that the amplitudes of the simulated ENSO events are much larger than that in the observations. In contrast to the comparable frequency between QQ and QB events for both El Niño and La Niña in the observations, the QB El Niño and QQ La Niña events are much more frequent than the QQ El Niño and QB La Niña in the simulations.

2.3 WACCM experiments

The monthly SST fields from the HadISST dataset (Rayner et al. 2003) over the period 1950–2010 were also used to derive the SST forcing fields for the WACCM experiment. Specifically, the control experiment was forced by the annual cycle of the monthly SST obtained for the period 1950–2010 (i.e., SST is a function of month but not of year). We ran the control experiment for 32 continuous years and used the last 30 years to obtain a reference state of the seasonal evolution of the atmospheric circulation without ENSO forcing. The circulation anomalies for each of the following sensitivity experiments are all relative to this reference state. We carried out four sensitivity experiments: QQ-El Niño, QQ-La Niña, QB-El Niño, and QB-La Niña, which were forced with the SST forcing fields that were constructed by imposing the evolving SST anomaly fields in the tropics (30°S–30°N)

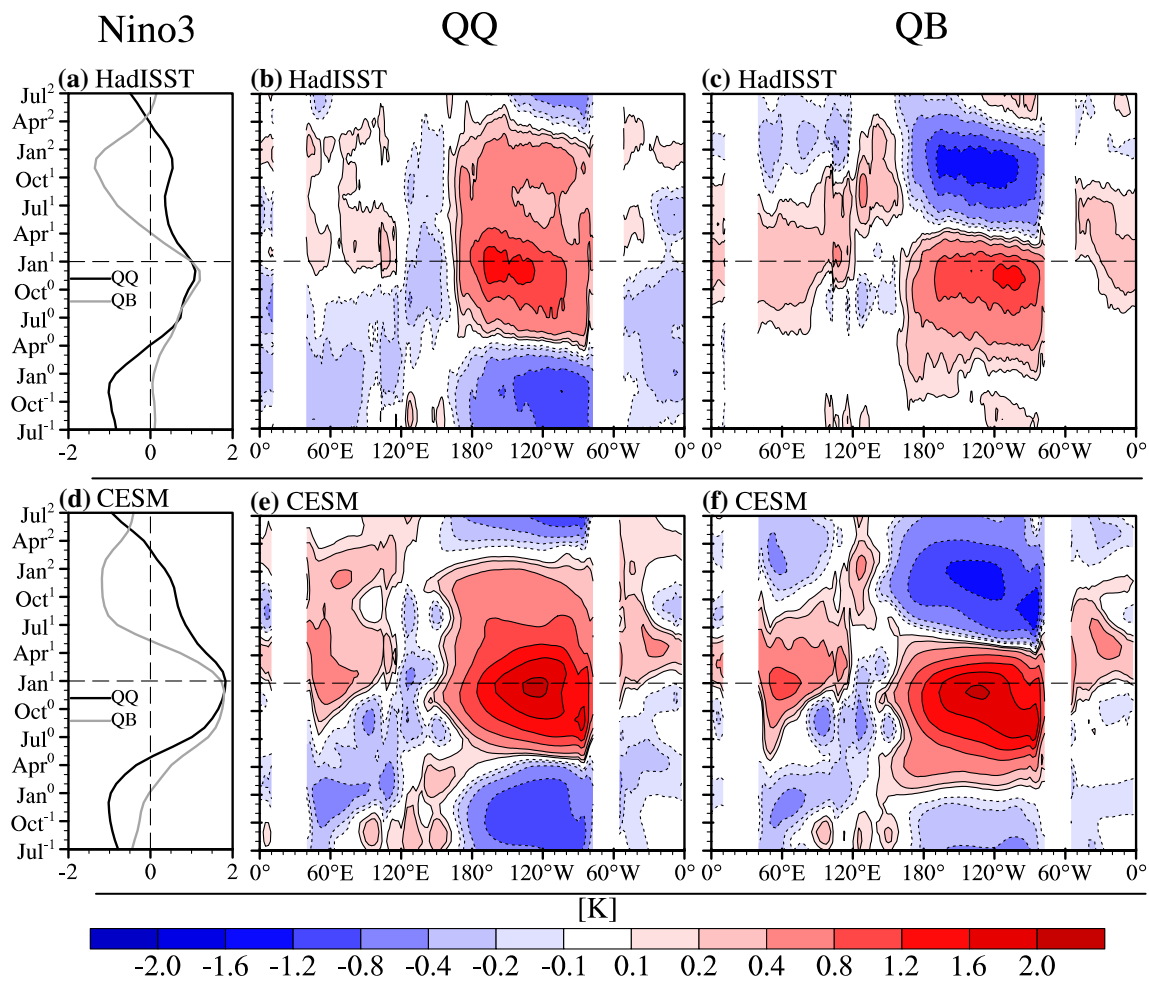


Fig. 1 Seasonal evolution of the warm-minus-cold composite **a, d** Niño3 index and **b, c, e, f** the composite equatorial (5°S–5°N) temperature (SST) anomalies for the quasi-quadrennial (QQ; black in **a** and **d, b** and **e**) ENSO and quasi-biennial (QB; gray in **a** and **d, c** and **f**) ENSO, from (top) the HadISST and (bottom) the NCAR CESM-WACCM

Table 2 List of the CMIP5 experiments from CESM1-WACCM

Experiment	Description
piControl	200-years, external forcings fixed at 1850
Historical-R1	156-years, observed external forcings during 1850–2005
Historical-R2–7	51-years, observed external forcings during 1955–2005, with different initial conditions.

The total length of the dataset is 662 (= 200 + 156 + (51 × 6)) years

Table 3 List of ENSO events in the CMIP5 simulations from CESM1-WACCM

ENSO type	Case number	Composite Niño3 amplitude (K)
El Niño	QQ 25	1.95
	QB 85	2.08
La Niña	QQ 87	-1.71
	QB 21	-1.54

on the climatological SST annual cycle for each of the four experiments. The monthly SST anomaly fields from the developing year (superscript “0”) to the decaying year (superscript “1”) of ENSO events, and to the summer of the next year (superscript “2”) after the ENSO decay year were obtained (30 months) from the lead–lag composite of the SST anomalies for all of the QQ-El Niño, QQ-La Niña, QB-El Niño, and QB-La Niña events identified between 1950 and 2012 (also see Fig. 1). Forced by the temporally

varying SST fields, each experiment was restarted every 30 months (Jan⁰–Jun²) and run 30 times with different initial conditions; the ensemble means were used for the following composite analysis of the circulation responses.

3 QQ and QB ENSO in the observations and CESM1

To demonstrate the differing evolution of ENSO SST anomalies between QQ and QB events, we show in Fig. 1 the seasonal evolution of the warm-minus-cold composite Niño3 index and the composite SST anomalies in the tropics (5°S–5°N) for the QQ and QB ENSO, respectively, and from HadISST and CESM, respectively. While the QQ ENSO, on average, always begins to develop in the early time of year 0, matures in the following winter season (year 0–year 1), and decays slowly until the next winter (year 1–year 2), the QB ENSO tends to mature slightly earlier than the QQ ENSO; then it decays rather quickly in its decaying year, and gets reversed before the summer (year¹); it is even followed by a mature ENSO of the opposite polarity until the next winter season (year 1–year 2; Fig. 1a–c). The remarkably contrasting seasonal evolutions of ENSO between the QQ and QB events are fairly consistent between the HadISST data and CESM1 (Fig. 1a–c vs. Fig. 1d–f). The composite peak intensities for both the QQ and QB ENSO are considerably stronger in CESM than in HadISST (Tables 1, 3). The much stronger SST anomalies in the tropical eastern Pacific in CESM than those in HadISST are associated with the much stronger SST anomalies in the tropical Indian Ocean in the winter-to-spring of the ENSO decay year in CESM (Fig. 1e, f vs. b, c; also see Li et al. 2012; Rao and Ren 2016).

As shown in Table 1, the number of QQ ENSO events recorded over the past 60 years is similar to the number of QB ENSO events recorded (i.e., warm: seven and nine; cold: six and seven, respectively). The comparable frequencies of the QQ and QB ENSO in the observations, as well as the contrasting evolutions between the QQ and QB ENSO in both the observations and the model, manifest the complex variability of ENSO. They also indicate the need to consider the QQ and QB ENSO events separately when we investigate ENSO's effects on the stratosphere.

4 Existence/non-existence of the delayed response of the stratosphere to QQ/QB ENSO in multi reanalysis datasets

4.1 Facts

The intensity of the circumpolar westerly jet in the northern winter stratosphere is a key indicator of the dominant

variability of winter stratospheric circulation in the extratropics. Figure 2 displays the lead-lag warm-minus-cold composite evolutions of the circumpolar (65°N–75°N) zonal wind anomalies from the summer of the ENSO developing year (July⁰) to the summer of the next year (July²) after the ENSO decay year (year “1”), for each of the three reanalysis datasets. The circumpolar zonal wind responses to ENSO are fairly consistent among the three datasets for both the QQ and QB ENSO. Specifically, the easterly responses of the stratospheric polar jet to a warm QQ ENSO are significant in both the concurrent winter of a mature ENSO and the next winter after the mature ENSO, and they tend to be relatively stronger and more significant in the next winter after mature ENSO (Fig. 2a, c, e, g). This clearly verifies the delayed stratospheric warming responses to ENSO identified by Ren et al. (2012) through linear regression of circulation anomalies against a 3–5 year timescale Niño3 index. However, the stratospheric easterly responses to a warm QB ENSO are confined to the current winter of a mature ENSO, and westerly responses begin to appear in the next winter associated with the reversed ENSO polarity (Fig. 2b, d, f, h). The remarkable contrasts of the stratospheric responses to the QQ ENSO and QB ENSO confirm the difficulties in identifying the significant delayed stratospheric responses when only a limited number of ENSO cases are used. Nevertheless, by considering the QQ and QB ENSO types separately in the three reanalysis datasets, we have demonstrated the robust existence/non-existence of the significant and delayed response of the extratropical stratosphere to the QQ/QB ENSO.

To further confirm the existence/non-existence of the delayed stratospheric response to the QQ/QB ENSO, Fig. 3 presents the corresponding polar temperature responses in the stratospheric layer during ENSO events. Also consistent among the three reanalysis datasets, the significant polar warming responses to a warm QQ ENSO appear in both the concurrent and the next winters with respect to the mature ENSO phase. In addition, the warming signals seem to always appear first in the midlatitudes since the leading spring or summer season, and persist until the winter of the polar warming (Fig. 3a, c, e, g). This is again in agreement with the poleward propagation of the ENSO-related circulation anomalies identified by Ren et al. (2012) for the ENSO with a periodicity of 3–5 years. In particular, after the mature phase of ENSO in the spring–summer of the ENSO decay year (year 1), there exist persistent and significant warming signals in the midlatitude stratosphere, which are even stronger and more significant than the midlatitude warming signals in the summer of the ENSO developing year. These significant warm signals in the midlatitude stratosphere were found intimately coupled with the delayed

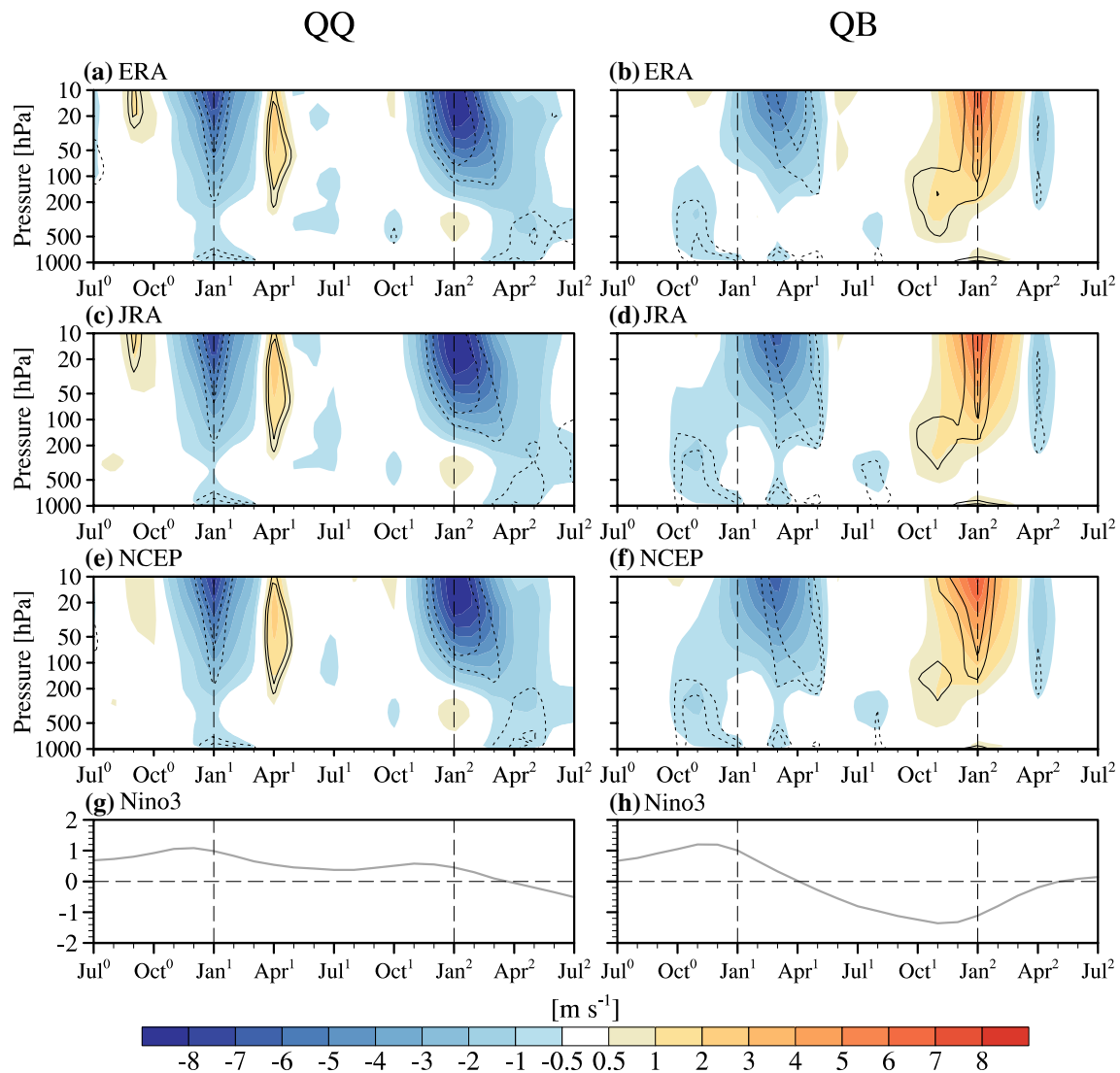


Fig. 2 Pressure-time cross-sections of the warm-minus-cold composite circumpolar (65°N – 75°N) westerly anomalies (m s^{-1} ; shading) in the Northern Hemisphere for (left) the QQ and (right) the QB ENSO from the a, b ERA, c, d JRA, and e, f NCEP/NCAR reanalysis data-

sets. Contours indicate the wind anomalies that are statistically significant at the 90 and 95 % levels. The *gray lines* in the bottommost panels denote the seasonal evolution of the composite Niño3 index

atmospheric responses in the tropical and midlatitude troposphere (Ren et al. 2012; Rao et al. 2014), that in turn were related to the 1–2 seasons delayed responses of other tropical oceans to the ENSO signals in the Pacific (Newell and Weare 1976; Angell 1981; Reid et al. 1989; Yulaeva and Wallace 1994; Kumar and Hoerling 2003; Lau et al. 2005). Figures 4 and 5 will show further evidence of the vertically and meridionally coupled thermal atmospheric responses to QQ ENSO during the ENSO decay years.

In accordance with Fig. 2, the polar stratospheric warming responses to a warm QB ENSO are also confined to the concurrent winter–spring season of the mature ENSO phase, and there are reversed polar cooling responses in the next winter associated with the reversed polarity of ENSO (Fig. 3b, d, f, h). Based on this finding, we next will focus mainly on the QQ ENSO to demonstrate the dynamical linkage between the tropical ENSO forcing and the delayed responses in the extratropical stratosphere in the next winter after mature ENSO phase.

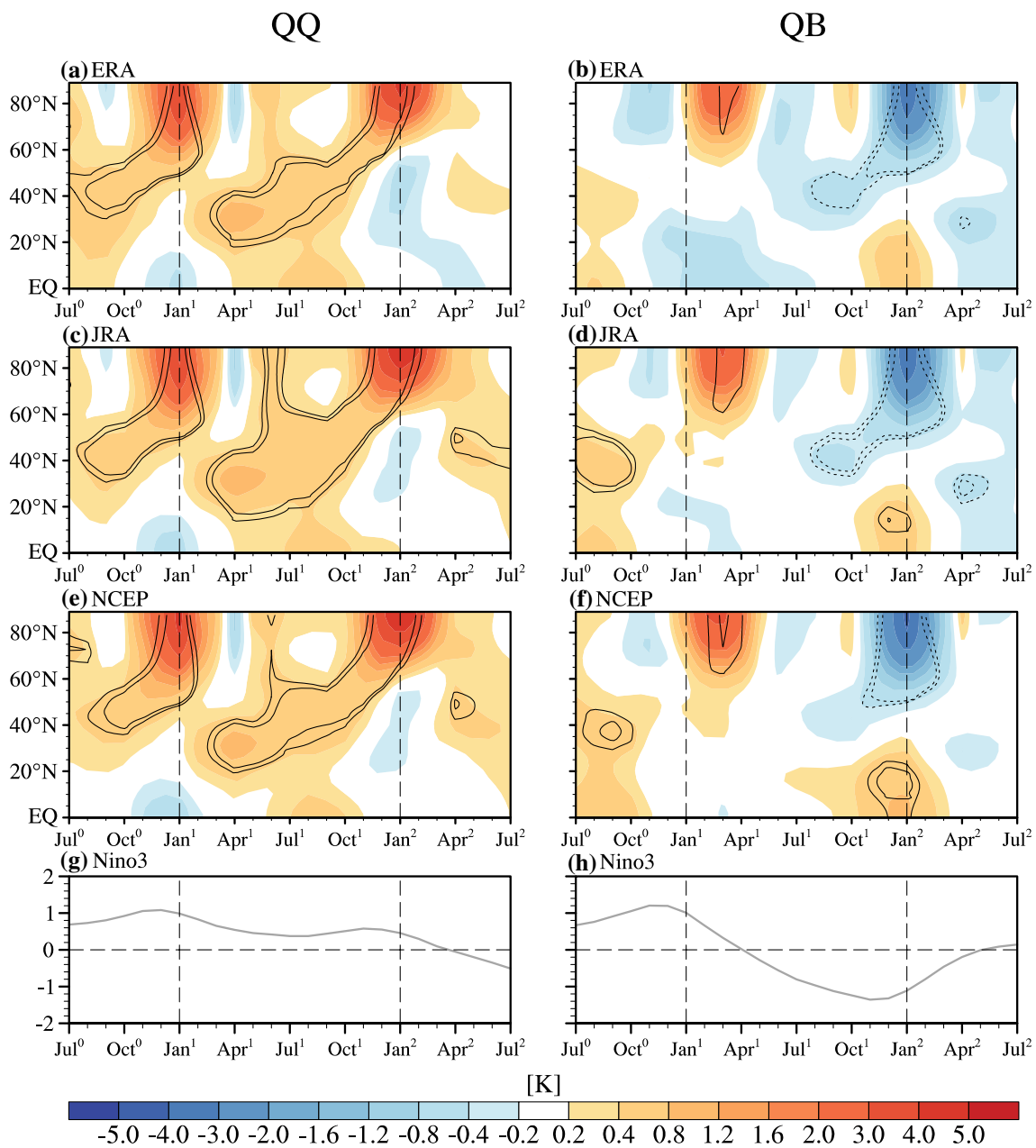


Fig. 3 As in Fig. 2, but for the latitude-time cross-sections of the composite temperature anomalies (K) in the northern stratospheric layer (150–20 hPa)

4.2 Dynamical linkage of QQ ENSO to the stratospheric responses in the next winter after mature ENSO

4.2.1 Vertical and meridional coupling of the delayed atmospheric responses following a mature ENSO

Figure 4 shows the temperature anomaly patterns in the stratospheric layer (150–20 hPa) for the concurrent winter, the following spring and summer, and the next winter

after a mature QQ ENSO. It is consistent among the three reanalysis datasets that, after the polar stratospheric warming in the concurrent winter of a mature warm QQ ENSO (leftmost panels in Fig. 4), zonally quasi-homogeneous warm temperature anomalies develop in the midlatitudes that persist from the following spring into the summer months (two middle columns in Fig. 4), and are followed by significant polar stratospheric warming in the next winter after mature ENSO (rightmost panels in Fig. 4). Also, as demonstrated by Ren et al. (2012), the three reanalysis

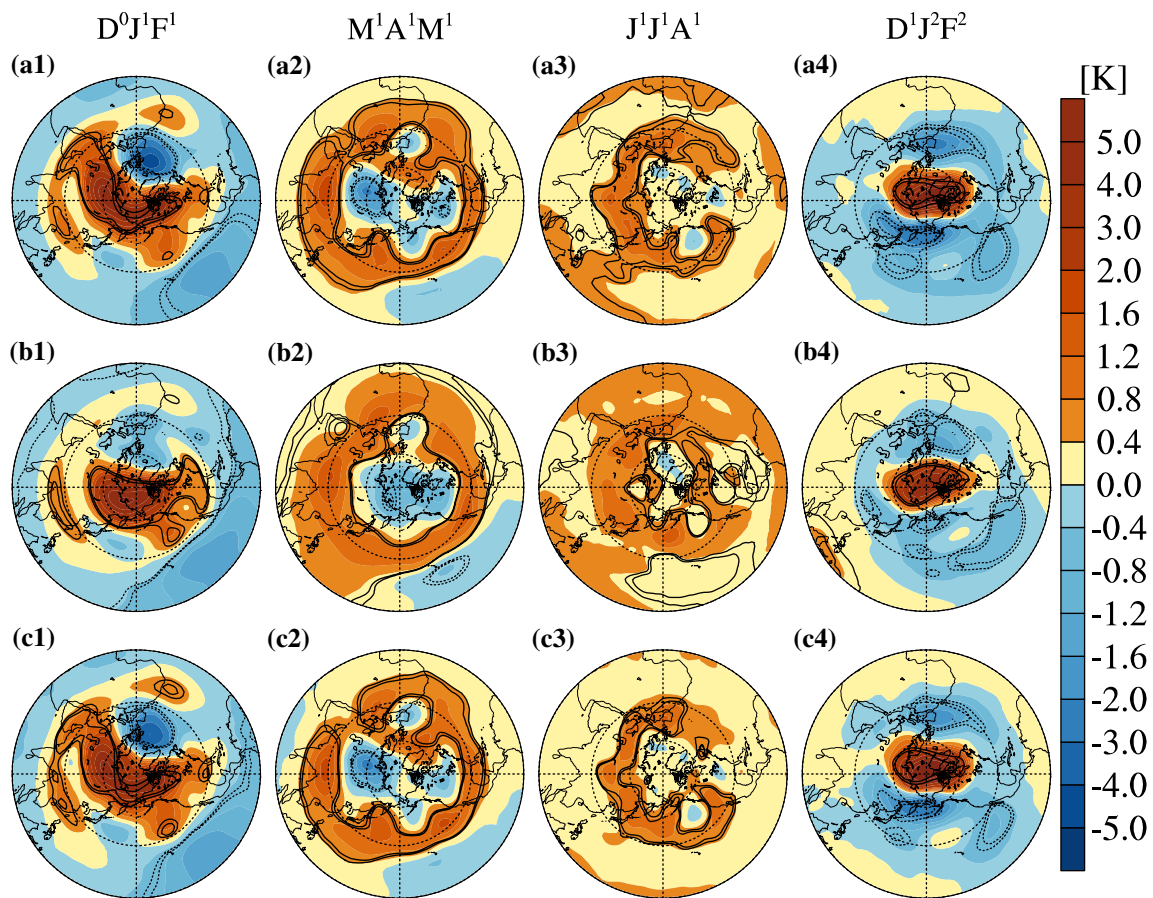


Fig. 4 Lead-lag composite patterns of temperature anomalies in the stratospheric layer (150–20 hPa) in (*leftmost column*) the concurrent winter ($D^0J^1F^1$), (*second left column*) the following spring ($M^1A^1M^1$), (*third left column*) the following summer ($J^1J^1A^1$), and (*rightmost*

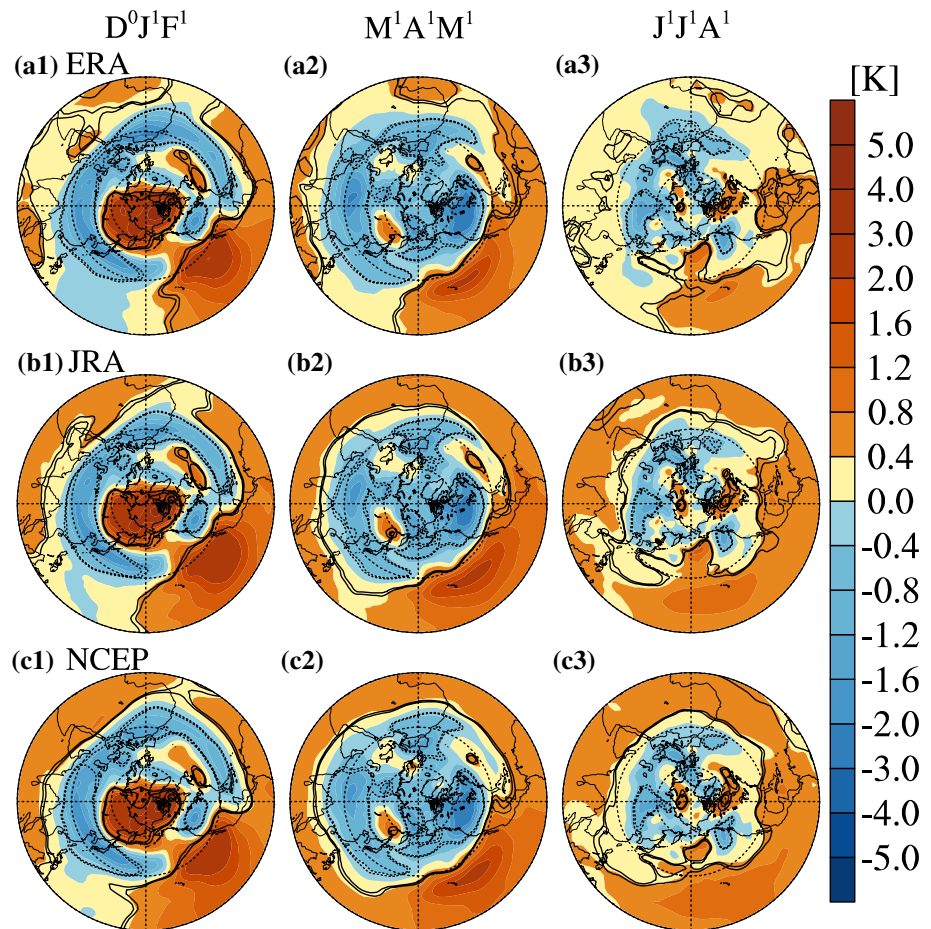
column) the next winter ($D^1J^2F^2$) with respect to the mature phase of a warm QQ ENSO in the (*top*) ERA, (*middle*) JRA, and (*bottom*) NCEP/NCAR reanalysis datasets. Contours indicate temperature anomalies that are statistically significant at the 90 and 95 % levels

datasets consistently show that the persistent and zonally quasi-homogeneous warm temperature anomalies in the midlatitude stratosphere are coupled with the persistent and zonally quasi-homogeneous cold temperature anomalies in the midlatitude troposphere since the concurrent winter (Fig. 5). These zonally homogeneous cold (or negative geopotential height) anomalies in the midlatitude troposphere have been known to be coupled to the warm (or positive geopotential height) anomalies in the tropics, both of which tend to become zonally homogeneous in response to the zonally quasi-homogeneous SST anomalies caused by the delayed SST responses over the tropical Indian Ocean and Atlantic since the winter–spring after a mature ENSO (Enfield and Mayer 1997; Klein et al. 1999; Saravanan and Chang 2000; Kumar and Hoerling 2003; Lau et al. 2005).

To demonstrate the intimate coupling of the atmospheric responses to ENSO between the tropics and extratropics, and between the troposphere and stratosphere, Fig. 6 displays the pressure–time evolution of the zonal-mean temperature anomalies in the tropics, in the midlatitudes, and in

the polar region. The three reanalysis datasets consistently show that in the tropics (Fig. 6a, d, g), significant warm responses in the troposphere appear from November of the mature warm ENSO winter (Nov^0) and persist throughout the ENSO decay year; and these responses are coupled to weaker cold anomalies in the lower tropical stratosphere. This vertical coupling of the thermal anomalies clearly indicate the decreased thickness of the atmospheric layer in the lower stratosphere as a direct response to the increased thickness of the tropospheric layer that was caused by the anomalous tropical convective heating by ENSO (Ren et al. 2012). In the midlatitudes (Fig. 6b, e, h), on the other hand, cold anomalies in the troposphere are vertically coupled with warm anomalies in the stratosphere, which prevails during the summer–autumn of the ENSO developing year. In the spring and summer following a mature ENSO, this vertical thermal coupling appears again and persists through the following autumn, although the tropospheric cold anomalies are much weaker than the previous year and are confined in the upper troposphere. Following the

Fig. 5 As in Fig. 4, but for the temperature anomalies at 200 hPa in (*left column*) the concurrent winter ($D^0J^1F^1$), (*middle column*) the following spring ($M^1A^1M^1$), and (*right column*) the following summer ($J^1J^1A^1$)



significant warming in the midlatitude stratosphere, significant warm anomalies appear in the polar stratosphere in both the concurrent winter of a mature ENSO and the following winter, which always appear earlier in the upper layer and exhibit a clear downward propagation (Fig. 6c, f, i). Also in agreement with Fig. 2, the polar warming anomalies in the next winter are slightly stronger, and exhibit a deeper vertical structure, compared with that in the concurrent winter.

4.2.2 Anomalous wave activity in the concurrent and the next winters

In addition to the warm temperature anomalies that develop in the midlatitude stratosphere before the winter season, anomalous planetary wave activity is expected to induce anomalous meridional exchanges and cause stratospheric polar warming in both the concurrent and the next winter after a mature ENSO. To demonstrate the ENSO-related wave responses from the troposphere to the stratosphere, we first show in Fig. 7 the geopotential height responses as well as the 3D E–P flux (Plumb 1985) responses during both winters. The three reanalysis datasets consistently

show that, during the concurrent winter of a mature ENSO (Fig. 7a, c, e), a PNA-like wave train is the dominant pattern in the upper troposphere, which originates from the tropical eastern Pacific (positive height responses), goes through the northeastern Pacific (negative height responses), and gets into North America (positive height responses). The E–P flux vectors also clearly indicate that the wave train is initiated from the tropical eastern Pacific region. Associated with the PNA wave train responses, the geopotential height responses also tend to exhibit zonally quasi-homogeneous distributions that are consistent with the temperature responses shown in Fig. 5. Moreover, on top of the zonally quasi-homogeneous nature of this response, the geopotential height responses induce a generally anomalous wavenumber-1 pattern in the extratropics, with negative anomalies straddling the north Eurasian continent and the northern Pacific, while positive anomalies extend across North America and the North Atlantic region. More importantly, the vertical component of the wave flux anomalies (shading in Fig. 7) indicates that in the concurrent winter of a mature ENSO, upward propagation of wave energy appears in the extratropics along the zone with a strong meridional height gradient and where

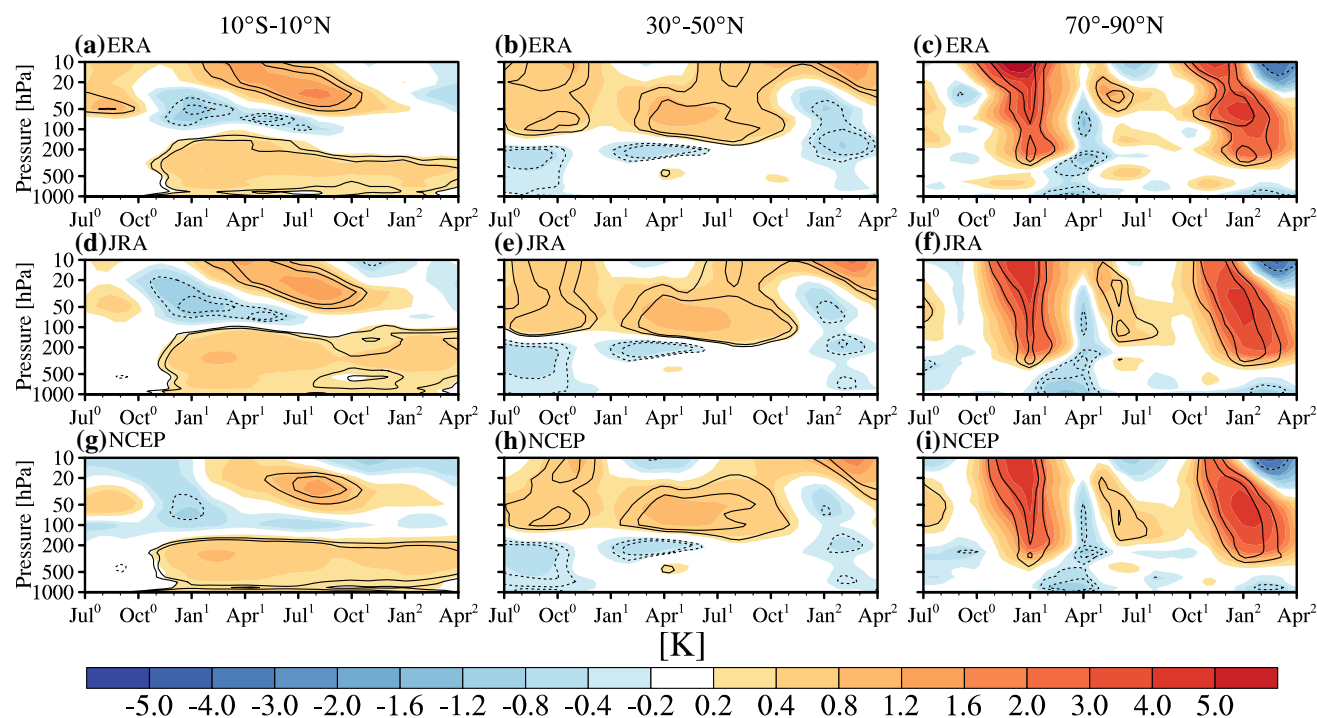


Fig. 6 Pressure-time cross-sections of the warm-minus-cold composite temperature anomalies (K; shading) in (*left*) the tropics (10°S – 10°N), (*middle*) the midlatitudes (30°N – 50°N), and (*right*) the polar region (70°N – 90°N), from the preceding summer (July⁰) of the

QQ ENSO developing years to the next spring after the QQ ENSO decay years (April²). Contours indicate temperature anomalies that are statistically significant at the 90 and 95 % levels

the E–P flux tends to be poleward from the negative to the positive height response regions. Obviously, the most significant upward propagation is found over the northeastern Pacific region between the negative lobe of the PNA over the North Pacific and the second positive lobe of the PNA over North America.

In the winter after a mature warm ENSO (Fig. 7b, d, f), the PNA wave pattern tends to diminish associated with the diminishing warm ENSO signals in the tropics. However, poleward wave flux anomalies, though much weaker, can still be identified from the tropical Pacific to the extratropics. In addition, the geopotential height responses in the extratropics no longer exhibit a wavenumber-1 pattern, as in the previous winter, but show a general wavenumber-2 pattern. An anomalous upward wave flux is still evident in the extratropics, but the strongest upward propagation has been shifted to North Atlantic and the Greenland regions. Again, these features are largely consistent among the three reanalysis datasets.

To further show the ENSO-related planetary wave patterns in the stratosphere in both winters, Fig. 8 displays the vertical distributions of the geopotential height responses averaged over the 45°N – 75°N latitude band. In the concurrent winter of a mature warm ENSO (Fig. 8a, c, e), the anomalous geopotential height pattern in the stratosphere indeed exhibits a general wavenumber-1 form that

is associated with the wavenumber-1 pattern in the upper troposphere (i.e., the PNA-related response). By referring to the winter climatology of the zonal deviation of geopotential height, it is seen that the wave pattern, including the height ridge around the Aleutian region and the trough over the North Atlantic, is clearly intensified in the stratosphere during the concurrent winter of a mature warm ENSO. In contrast, connected to the anomalous wavenumber-2 pattern in the upper troposphere, the geopotential height responses in the stratosphere also show a general wavenumber-2 pattern in the next winter season after a mature warm ENSO (Fig. 8b, d, f). Obviously, the climatological trough over the North Atlantic is anomalously deepened by the anomalous wave pattern although the Aleutian ridge is weakened.

To explicitly demonstrate the dynamical contributions of the anomalous planetary waves to the stratospheric polar warming during the two winters, Fig. 9 shows the temporal evolution of the E–P flux and its divergence anomalies in the extratropics (60°N – 80°N ; Fig. 9a, d, g), and the corresponding components contributed by the anomalous wavenumber-1 (Fig. 9b, e, h), and wavenumber-2 (Fig. 9c, f, i). Associated with the polar warming anomalies in the concurrent winter as well as in the next winter after a mature warm ENSO, an anomalous upward E–P flux and its convergence into the stratosphere above 200 hPa prevail during

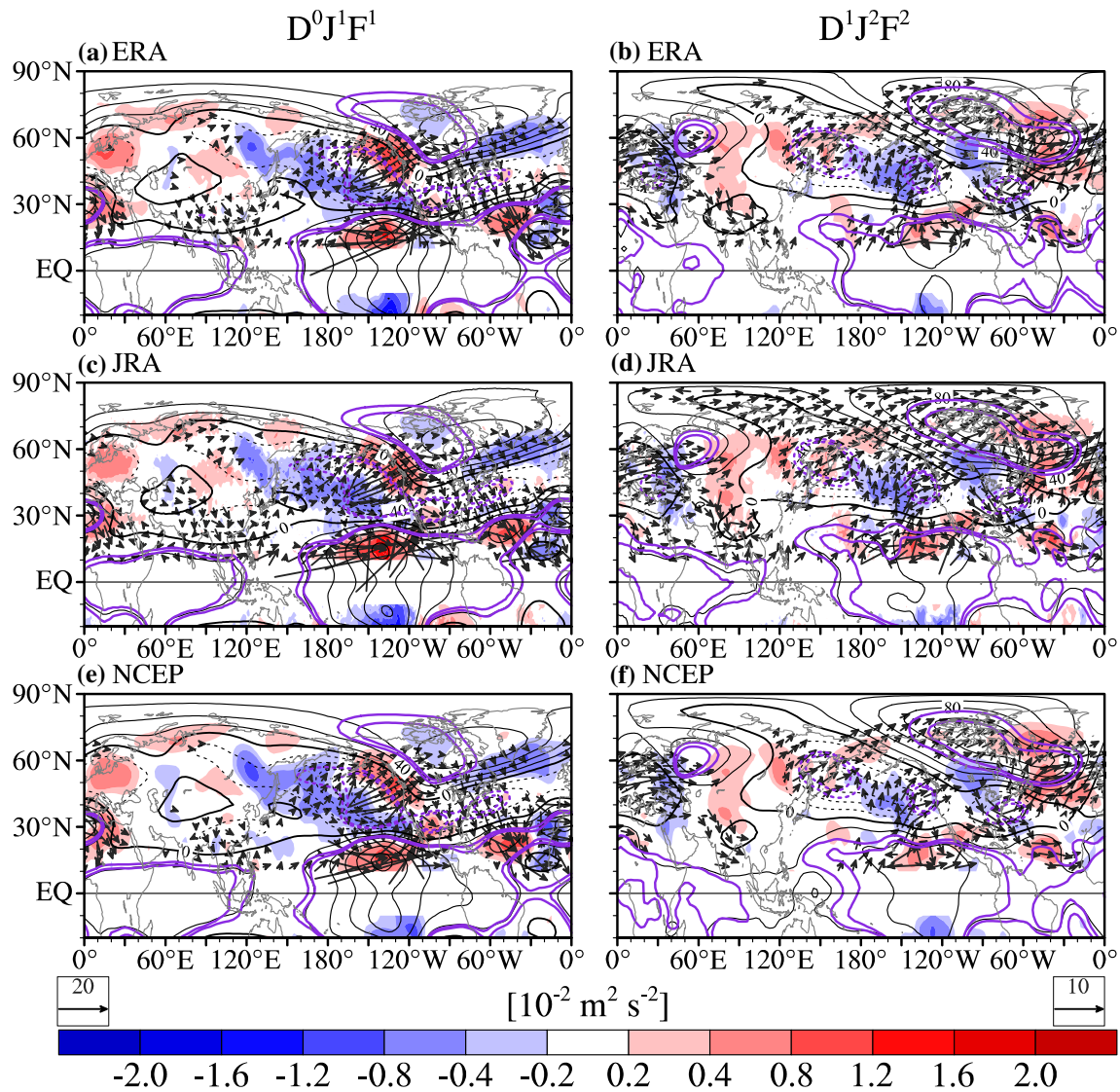


Fig. 7 Warm-minus-cold composite 3D wave flux anomalies at 200 hPa (*left*) in the concurrent winter of a mature QQ ENSO ($D^0J^1F^1$) and (*right*) the next winter after a mature QQ ENSO ($D^1J^2F^2$), from the (*top*) ERA, (*middle*) JRA, and (*bottom*) NCEP/NCAR reanalysis datasets. Vectors represent the *horizontal* compo-

ponents ($m^2 s^{-2}$) and *shading* denotes the vertical ($10^{-2} m^2 s^{-2}$) components. The *black contours* are the composite geopotential height anomalies (m) at 200 hPa. *Purple contours* indicate height anomalies that are statistically significant at the 90 and 95 % level

both winters (Fig. 9a, d, g). Despite the wavenumber-2 wave pattern in the extratropical stratosphere in the next winter as shown in Figs. 7 and 8, the anomalous upward wave flux and its convergence seem to be always dominated by the wavenumber-1 component in both winters (Fig. 9a, d, g vs. 9b, e, and h). However, we note that the E–P flux convergence caused by the consistently upward flux of wavenumber-1 tends to be mainly confined to the middle and upper stratosphere (Fig. 9b, e, h), or only around January in NCEP/NCAR (Fig. 9h), and the total E–P flux convergence in the lower stratosphere seems to be mainly contributed by wavenumber-2, especially in NCEP/NCAR. The wavenumber-2 E–P flux components tend to

be significantly downward in the upper stratospheric layer and results in the E–P flux convergence (divergence) in the lower (mid–upper) stratosphere (Fig. 9c, f, i). Moreover, the high degree of consistency among the three reanalysis datasets, in terms of indicating the anomalous planetary-wave activity in the two winters following a mature ENSO, essentially confirms that planetary wave activity is anomalously stronger in both winters and is generally dominated by the planetary wavenumber-1/wavenumber-2 in the upper/lower stratosphere. The three reanalysis datasets also consistently show that, the zonal wave pattern in the stratosphere is generally dominated by wavenumber-1 in the concurrent winter of a mature ENSO, but by wavenumber-2 in

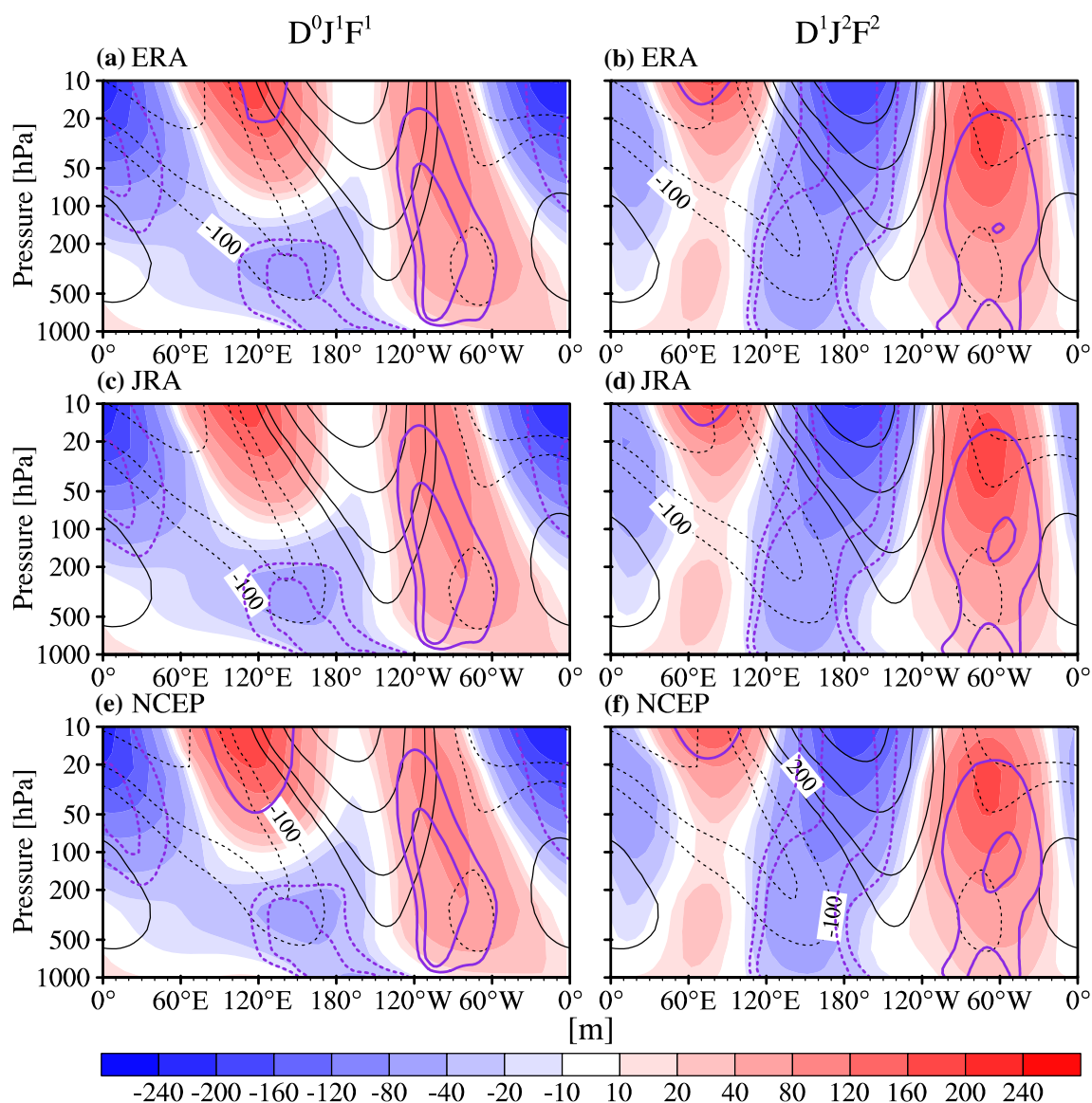


Fig. 8 As in Fig. 7, but for the pressure-longitude distributions of the composite geopotential height anomalies (m; shading) and the zonal deviations of the climatological mean geopotential heights (m; black

contours) averaged over the 45°N–75°N latitude band. Purple contours indicate composite height anomalies that are statistically significant at the 90 and 95 % levels

the next winter after mature ENSO, as already indicated by Ren et al. (2012).

5 Modeling evidence of the delayed stratospheric response to QQ ENSO

5.1 Existence/non-existence of the delayed stratospheric response to QQ/QB ENSO in model simulations

In this section, we use the long-term CMIP5 simulations from a fully coupled ESM (CESM1-WACCM), and the

general circulation model (GCM) WACCM to provide modeling evidence of the existence of ENSO's delayed effects on the extratropical stratosphere. Figure 10 shows the warm-minus-cold composite circumpolar zonal wind anomalies for QQ and QB ENSO events from the CESM1-WACCM simulations and those from the sensitivity experiments of WACCM forced by the QQ and QB ENSO SST anomalies. The circumpolar zonal wind responses in the models are similar to those in the reanalysis data, clearly showing significant easterly responses in both the concurrent and the next winter following a mature QQ ENSO (Fig. 10a, c), but only in the concurrent winter of a QB ENSO (Fig. 10b, d). However, in

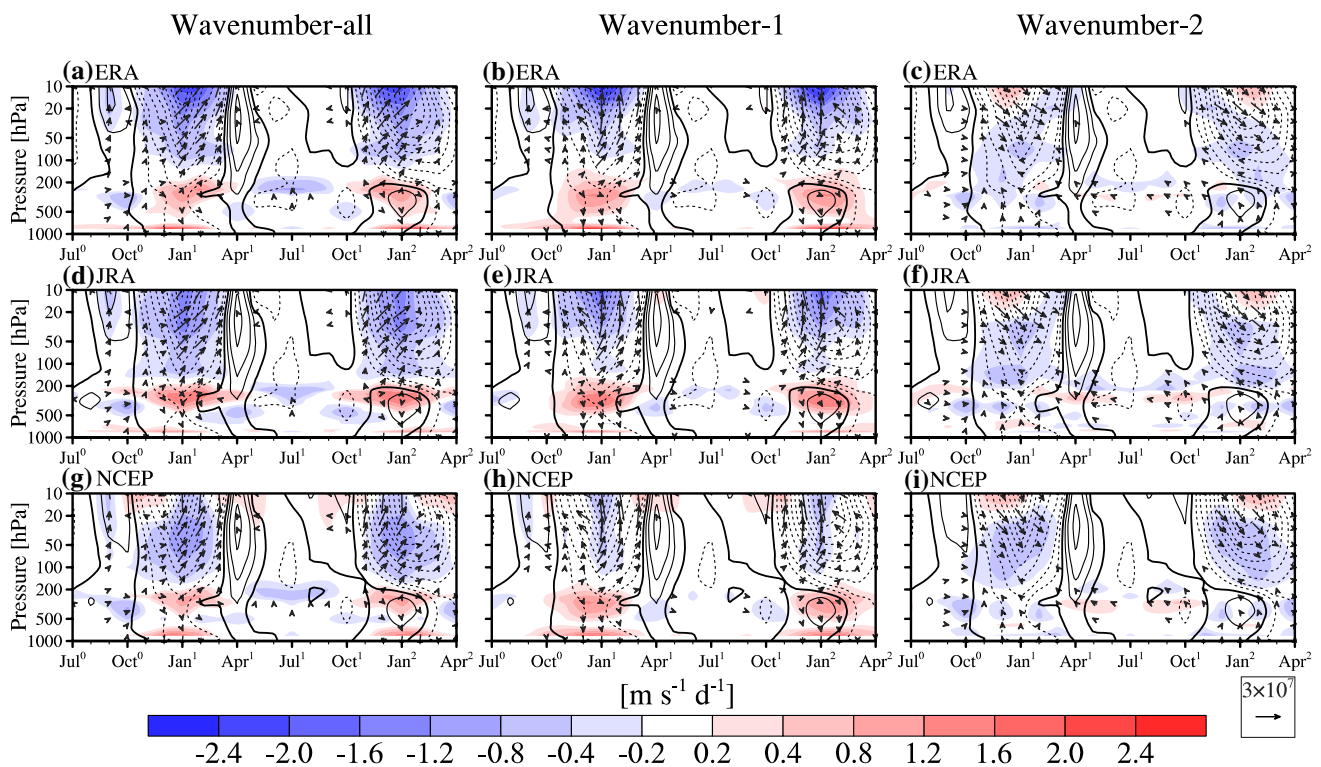


Fig. 9 Pressure-time cross-sections of warm-minus-cold composite E–P flux anomalies ($\text{m}^3 \text{s}^{-2}$; vectors, normalized by local air density) and their divergence ($\text{m s}^{-1} \text{d}^{-1}$; shading) in the circumpolar region (60°N – 80°N) by (left) all planetary-waves, (middle) the wavenum-

ber-1 component, and (right) the wavenumber-2 component from the (top) ERA, (middle) JRA, and (bottom) NCEP/NCAR reanalysis datasets. Contours indicate the composite circumpolar westerly anomalies (65°N – 75°N)

spite of the larger amplitudes of ENSO events in CESM1-WACCM (Tables 1 vs. 3), the simulated responses in the concurrent winter seem much weaker than those in the observations, especially for the QQ ENSO events (Figs. 10a, b vs. 2a, b). In addition, the easterly responses in the upper stratospheric layer appear much earlier in the early winter before January of year 1 (Jan^1) than they do in the observations. The upper stratospheric response tends to reverse its sign during the late winter of a mature QQ ENSO (Fig. 10a). The easterly response during the concurrent winter of QQ ENSO in the WACCM sensitivity experiment appears more persistent than that in the observations and that in the CESM1-WACCM simulations (Fig. 10c). As with the reanalysis data, we now focus mainly on the simulated dynamical processes that are responsible for the delayed responses of the stratosphere to QQ ENSO.

5.2 Simulated dynamical processes linking the QQ ENSO to its delayed effects on the stratosphere

Similarly as in Fig. 6, the pressure–time evolutions of the simulated temperature responses in the tropics, in the mid-latitudes, and in the polar region are displayed in Fig. 11.

Consistent with that in the reanalysis data, warm (cold) temperature anomalies persist in the tropical upper troposphere (lower stratosphere) from the ENSO-developing year to the next winter after the ENSO-decay year, and they are strongest during the winter–spring of the ENSO decay year (Fig. 11a, d). Coupled with these thermal anomalies, there are cold anomalies in the midlatitude troposphere and warm anomalies in the midlatitude stratosphere. These thermal anomalies persist from the concurrent winter of mature ENSO to the spring–summer of ENSO-decay years (Fig. 11b, e). Following the warm anomalies in the midlatitude stratosphere in summer of the ENSO-decay year for both CESM1-WACCM and WACCM, polar warming anomalies always appear again in the next winter after mature ENSO (Fig. 11c, f). Compared with that in the reanalysis data, the polar warming response in CESM1-WACCM appears earlier in the concurrent winter, and the temperature responses in the tropics and the mid-latitudes in the model simulations seem slightly stronger than in the reanalysis data, in relation to the larger ENSO amplitudes in CESM1-WACCM (Fig. 11a, b vs. the left and the middle columns in Fig. 6). However, the vertically coupled warm (cold) response centers in the midlatitude stratosphere (troposphere) seem to be at much lower levels and become

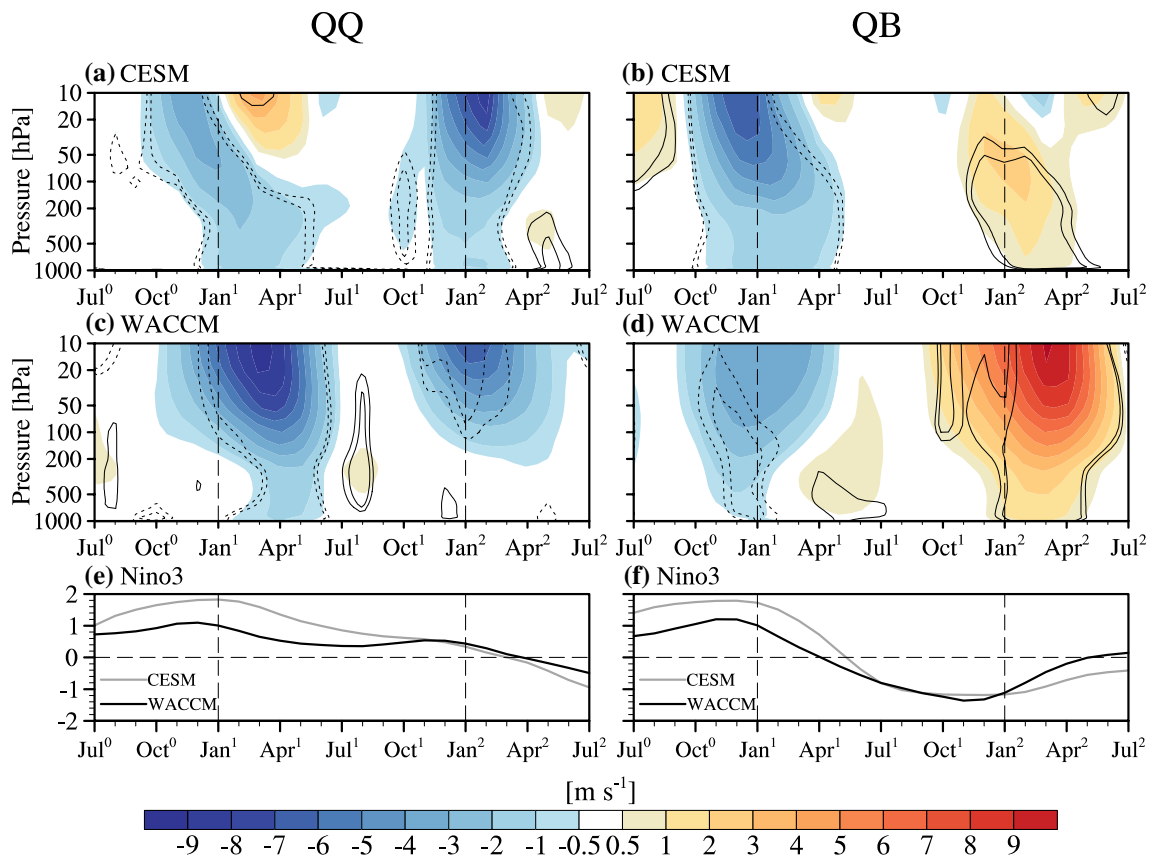


Fig. 10 As in Fig. 2, but for (top) the fully coupled model simulations from the NCAR CISM-WACCM and (bottom) the AGCM WACCM experiments forced by ENSO SST anomalies. The gray and

black lines in the bottommost panels indicate the Niño3 index from CISM-WACCM and the AGCM WACCM experiments, respectively

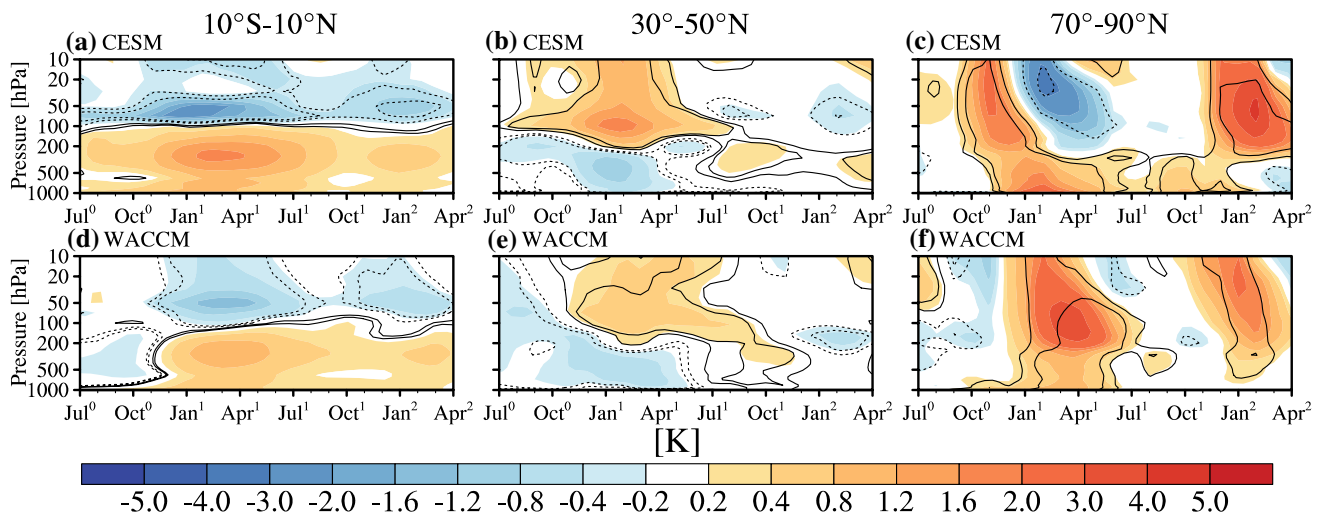


Fig. 11 As in Fig. 6, but for the temperature anomalies from (top) the fully coupled model simulations from the NCAR CISM-WACCM and (bottom) the AGCM WACCM experiments forced by the QQ ENSO SST anomalies

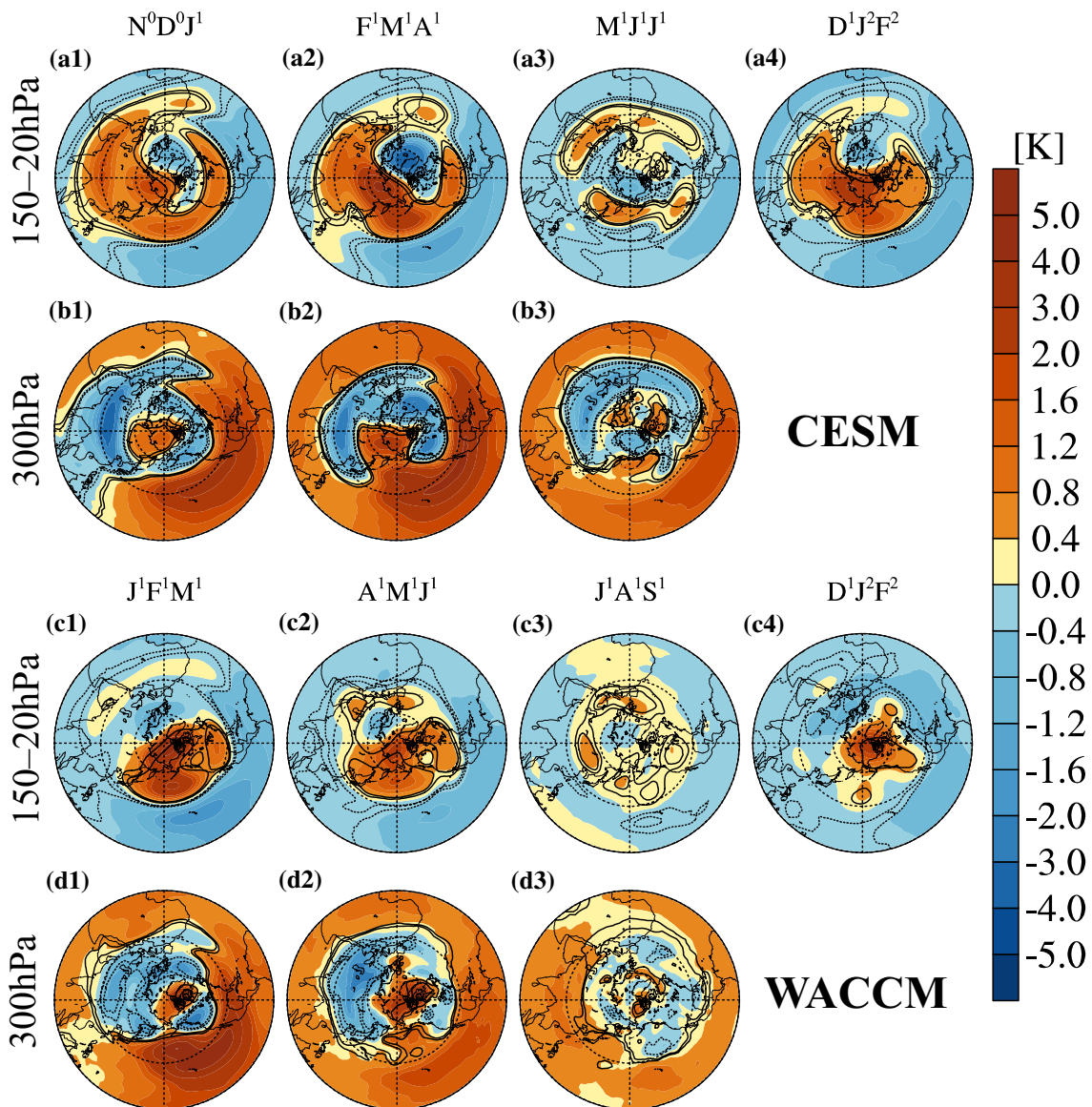


Fig. 12 As in Figs. 4 and 5, but for the 3-month mean temperature anomalies **a, c** in the stratospheric layer (150–20 hPa) and **b, d** in the upper troposphere (300 hPa), from **a, b** the fully coupled model simu-

lations from the NCAR CESM-WACCM and **c, d** AGCM WACCM experiments forced by the QQ ENSO SST anomalies

much weaker till the summer of ENSO decay-year, compared with those in the reanalysis data (middle columns in Figs. 6 and 11).

Nevertheless, the simulated zonal patterns of the temperature responses in the stratosphere and troposphere in CESM1-WACCM (Fig. 12a, b) and in WACCM (Fig. 12c, d) still confirm that, in the spring–summer of ENSO-decay years (middle columns in Fig. 12), the vertically coupled temperature responses in the midlatitude stratosphere and troposphere are generally zonally homogeneous, and they are followed by the polar warming responses in the next winter after mature QQ ENSO (rightmost column in Fig. 12).

To understand the existing polar warming and the easterly circumpolar wind responses in both winters following a mature QQ ENSO, the planetary wave responses in the extratropics are shown in Fig. 13 in terms of the pressure–longitude geopotential height anomaly distributions during the two winter seasons. During the concurrent winter of a QQ ENSO, both models indicate strengthened wavenumber-1 patterns from the upper troposphere to the stratosphere (Fig. 13a, c), particularly for the WACCM experiment (Fig. 13c). In the next winter, however, although the wavenumber-2 is present in the reanalysis data (right panels in Fig. 8), the models still show a general wavenumber-1 pattern in the upper troposphere and the stratosphere,

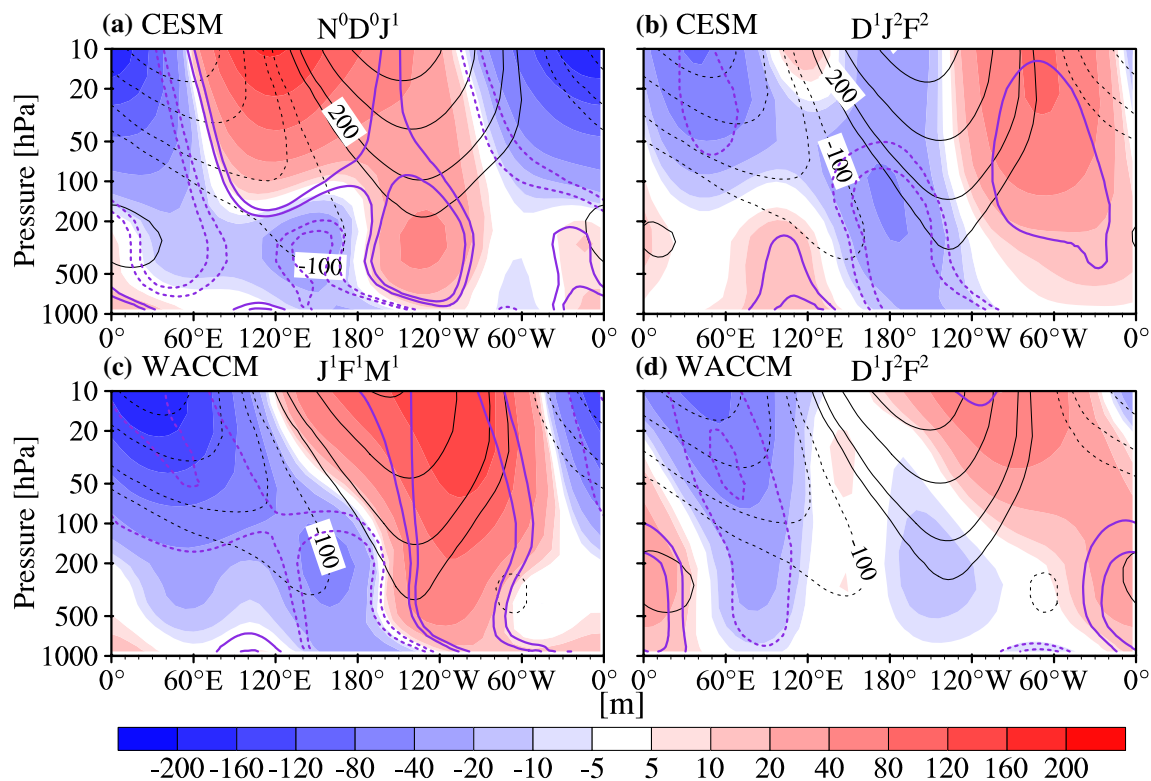


Fig. 13 As in Fig. 8, but for (top) the fully coupled model simulations from the NCAR CESM-WACCM and (bottom) AGCM WACCM experiments forced by the QQ ENSO SST anomalies

and they still tend to strengthen the climatological wave-number-1 (Fig. 13b, d).

The pressure–latitude patterns of the E–P flux responses shown in Fig. 14 further confirm that during the concurrent winter of a QQ ENSO, the upward E–P flux anomalies and their convergences in WACCM are stronger than those in CESM1-WACCM, corresponding to the much stronger easterly responses in the extratropics in WACCM (Fig. 14a, d); and they are indeed dominated by contributions from wavenumber-1 for both models (Fig. 14b, e vs. Figure 14c, f). During the next winter after a mature QQ ENSO, while the upward E–P flux anomalies and their convergences in WACCM are co-contributed by wavenumber-1 and wavenumber-2 (Fig. 14j–l), those in CESM1-WACCM are still dominated by wavenumber-1 in association with the wave-number-1 pattern in Fig. 13b.

6 Summary and discussion

6.1 Summary

By using three reanalysis datasets and the long-term simulation data records from CESM1-WACCM, as well as by performing a series of sensitivity experiments with

WACCM, this study has confirmed the existence of the delayed response of the extratropical stratosphere to QQ ENSO. We have demonstrated that, only when ENSO events decay quickly and are reversed during JAS of the ENSO-decay years are the effects of ENSO confined within the concurrent winter of a mature ENSO. The presence of the delayed polar warming/cooling responses in the next winter after a mature warm/cold ENSO is always associated with persistent and zonally quasi-homogeneous temperature anomalies in the midlatitude stratosphere from the spring to the summer of the ENSO-decay years. These anomalies are part of the zonally quasi-homogeneous, vertically and meridionally coupled thermal responses of the atmosphere from the tropics to the midlatitudes, and from the upper troposphere to the lower stratosphere. The zonally quasi-homogeneous thermal responses are in turn connected to the zonally quasi-homogeneous tropical SST forcing caused by the delayed SST responses over the tropical Indian and Atlantic oceans via the ENSO-induced anomalous zonal Walker circulation (Enfield and Mayer 1997; Klein et al. 1999; Saravanan and Chang 2000; Kumar and Hoerling 2003; Lau et al. 2005; Ren et al. 2012).

During the concurrent winter of a mature ENSO, while the ENSO forcing induces a dominant PNA pattern in the troposphere, an anomalous wavenumber-1 pattern prevails

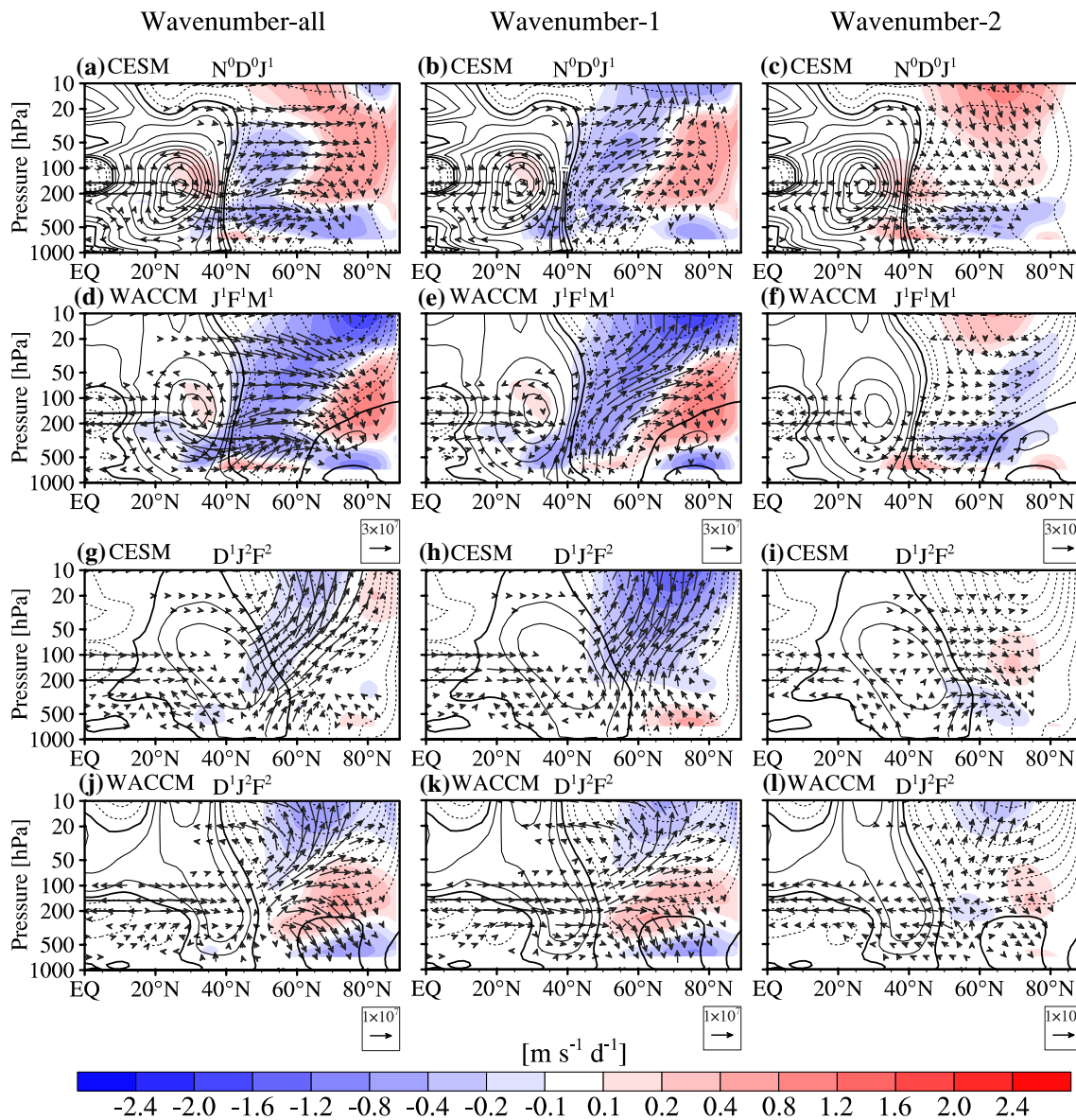


Fig. 14 Warm-minus-cold composite E–P flux anomalies ($\text{m}^3 \text{s}^{-2}$; vectors, normalized by local air density) and their divergence ($\text{m s}^{-1} \text{d}^{-1}$; shading) by (left) all planetary-waves, (middle) the wavenumber-1 component, and (right) the wavenumber-2 component in

a–f the concurrent and g–l the next winter, from a–c, g–i the fully coupled model simulations from the NCAR CESM–WACCM and d–f, j–l AGCM WACCM experiments forced by the QQ ENSO SST anomalies

in the extratropics and penetrates from the troposphere to the stratosphere. This acts to intensify/weaken the climatological wave pattern and results in the anomalously strong/weak meridional exchange and thus the polar warming/cooling in the current winter of a mature warm/cold ENSO. During the next winter after the mature ENSO, while the ENSO forcing and the PNA pattern in the troposphere are diminishing, the anomalous wave pattern becomes a clear wavenumber-2 from the upper troposphere to the stratosphere. Although the E–P flux convergence in the extratropical stratosphere still tends to be dominated by the anomalous wavenumber-1 in the upper layer, it is dominated

mainly by the anomalous wavenumber-2 in the lower layer where only the wavenumber-2 E–P flux converges though it is mostly downwards in the stratosphere.

Relative to the stratospheric responses in the three reanalysis datasets, the responses to ENSO during the concurrent winter in CESM1–WACCM simulations are weaker and appear in earlier winter months, whereas those in the WACCM experiments seem to be slightly stronger and appear in later winter months. Other than this, the existence/non-existence of the delayed stratospheric effects of the QQ/QB ENSO, as well as the ENSO-induced thermal responses and the anomalous wave patterns in both the

concurrent and the next winters following a mature ENSO, are closely comparable with those in the reanalysis datasets. The only difference between the models and the reanalysis is that the simulated wavenumber-2 patterns are much weaker in the next winter after mature ENSO for both CESM1-WACCM and WACCM. As a result, the wavenumber-2 E–P flux convergence in the lower stratospheric layer is much weaker and makes a trivial contribution to the E–P flux convergence in the extratropical stratosphere, and the dominance of the wavenumber-1 component in the E–P flux convergence remains clear in the next winter after mature ENSO in the CESM1-WACCM and WACCM simulations.

6.2 Discussion

This study used warm-minus-cold composite analysis, rather than composites for warm and cold ENSO events separately, to demonstrate ENSO's significant effects on the extratropical stratosphere. We took this approach because we aimed to provide a general picture by using as many ENSO cases as possible, to demonstrate the coexistence of the concurrent and the delayed effects of ENSO in the concurrent and the next winters after a mature ENSO, and to show the existent/non-existent delayed effects of the QQ/QB ENSO on the extratropical stratosphere in the next winter. We have confirmed the opposite-signed stratospheric responses to ENSO between warm and cold ENSOs, although we did find that the concurrent stratospheric responses exhibit significant asymmetries between warm and cold ENSOs, as well as the strong nonlinearity of the responses for warm and cold ENSOs (two manuscripts by Rao and Ren revised to *Journal of Geophysical Research*). In a subsequent paper, we will also demonstrate the possible asymmetries of ENSO's delayed effects on the stratosphere in the next winter after mature ENSO.

Based on the decomposition of ENSO's effects in the concurrent winter, as reported by Rao and Ren (2016), we may attribute the weaker and earlier occurrence of the stratospheric responses in CESM-WACCM to the stronger cancelling effects by, on average, the greatly overestimated SST forcing in the tropical Indian Ocean since the spring of the ENSO-decay years (Fig. 1d, f). This suggests that the model reproducibility of the tropical SST anomalies in other ocean basins during ENSO events may be crucial as well for the reproducibility of ENSO's effects on the extratropical atmosphere in both the troposphere and stratosphere.

In addition, this study focused on canonical ENSO and did not explicitly consider the possible effects of central Pacific (CP) ENSO events which have been known much weaker than canonical ENSO events and exhibit large uncertainties in their influences on the stratosphere (Hegy

and Deng 2011; Garfinkel et al. 2012; Xie et al. 2012; Hegyi et al. 2014). Though weaker SST anomalies can be found over the tropical CP during the composite canonical ENSO cycle (e.g. Figure 1), the approximate orthogonal relationship between canonical ENSO and CP ENSO (as 1st and 2nd EOF mode) actually has limited the entanglement of CP signals in the stratosphere.

Different from the current study, some studies have emphasized the possible effects of stratospheric variations on the tropical ENSO (e.g. Vimont et al. 2001; Huang et al. 2012; Chen et al. 2013), which may reflect the other side of the coupling between ENSO and the stratospheric variability, and will not change the fact that ENSO is the dominant source of the interannual variabilities of the climate system.

Acknowledgments This work was jointly supported by research grants from the National Science Foundation of China (41575041, 41430533, and 91437105), a Chinese Academy of Sciences project (XDA11010402), and a China Meteorological Administration Special Public Welfare Research Fund (GYHY201406001). We thank the relevant agencies (i.e., NCEP/NCAR, the ECMWF, the JMA, and the UKMO/HC) for providing the three reanalysis datasets (NCEP/NCAR, ERA, and JRA) and the SST analysis datasets (HadISST and COBE) used in this study.

References

- Angell JK (1981) Comparison of variations in atmospheric quantities with sea surface temperature variations in the equatorial eastern Pacific. *Mon Weather Rev* 109:230–243. doi:10.1175/1520-0493(1981)109<0230:coviq>2.0.co;2
- Barnett TP (1991) The interaction of multiple time scales in the tropical climate system. *J Clim* 4:269–285. doi:10.1175/15200442(1991)004<0269:tiomts>2.0.co;2
- Bejarano L, Jin F-F (2008) Coexistence of equatorial coupled modes of ENSO. *J Clim* 21:3051–3067. doi:10.1175/2007jcli1679.1
- Calvo N, Giorgetta MA, Garcia-Herrera R, Manzini E (2009) Nonlinearity of the combined warm ENSO and QBO effects on the Northern Hemisphere polar vortex in MAECHAM5 simulations. *J Geophys Res* 114:D13019. doi:10.1029/2008jd011445
- Calvo N, Garcia RR, Randel WJ, Marsh DR (2010) Dynamical mechanism for the increase in tropical upwelling in the lowermost tropical stratosphere during warm ENSO events. *J Atmos Sci* 67:2331–2340. doi:10.1175/2010jas3433.1
- Camp CD, Tung KK (2007) Stratospheric polar warming by ENSO in winter: a statistical study. *Geophys Res Lett* 34:L14703. doi:10.1029/2006gl028521
- Chen W, Takahashi M, Graf H-F (2003) Interannual variations of stationary planetary wave activity in the north winter troposphere and stratosphere and their relations to NAM and SST. *J Geophys Res* 108:4797. doi:10.1029/2003jd003834
- Chen SF, Chen W, Yu B, Graf HF (2013) Modulation of the seasonal footprinting mechanism by the boreal spring Arctic Oscillation. *Geophys Res Lett* 40:6384–6389. doi:10.1002/2013gl058628
- Danabasoglu G, Bates SC, Briegleb BP, Jayne SR, Jochum M, Large WG, Peacock S, Yeager SG (2012) The CCSM4 ocean component. *J Clim* 25:1361–1389. doi:10.1175/jcli-d-11-00091.1
- Dee DP, Uppala SM, Simmons AJ et al (2011) The ERA-Interim reanalysis: configuration and performance of the data assimilation system. *Q J R Meteorol Soc* 137:553–597. doi:10.1002/qj.828

- Duchon CE (1979) Lanczos filtering in one and two dimensions. *J Appl Meteorol* 18:1016–1022. doi:10.1175/1520-0450(1979)018<1016:lfloat>2.0.CO;2
- Ebita A, Kobayashi S, Ota Y et al (2011) The Japanese 55-year reanalysis “JRA-55”: an interim report. *Sola* 7:149–152. doi:10.2151/sola.2011-038
- Enfield DB, Mayer DA (1997) Tropical Atlantic sea surface temperature variability and its relation to El Niño–Southern Oscillation. *J Geophys Res* 102:929–945. doi:10.1029/96jc03296
- Evtushevsky OM, Kravchenko VO, Hood LL, Milinevsky GP (2015) Teleconnection between the central tropical Pacific and the Antarctic stratosphere: spatial patterns and time lags. *Clim Dyn* 44:1841–1855. doi:10.1007/s00382-014-2375-2
- Eyring V, Waugh DW, Bodeker GE et al (2007) Multimodel projections of stratospheric ozone in the 21st century. *J Geophys Res* 112:D16303. doi:10.1029/2006jd008332
- Eyring V, Shepherd T, Waugh D (eds) (2010a) Stratospheric processes and their role in climate: SPARC report on the evaluation of chemistry-climate models. WCRP-132, WMO/TD-1526, SPARC Rep. 5, p 408. <http://www.sparc-climate.org/publications/sparc-reports/>
- Eyring V, Cionni I, Bodeker GE et al (2010b) Multi-model assessment of stratospheric ozone return dates and ozone recovery in CCM-Val-2 models. *Atmos Chem Phys* 10:9451–9472. doi:10.5194/acp-10-9451-2010
- Garcia RR, Marsh DR, Kinnison DE, Boville BA, Sassi F (2007) Simulation of secular trends in the middle atmosphere, 1950–2003. *J Geophys Res* 112:D09301. doi:10.1029/2006jd007485
- García-Herrera R, Calvo N, Garcia RR, Giorgetta MA (2006) Propagation of ENSO temperature signals into the middle atmosphere: a comparison of two general circulation models and ERA-40 reanalysis data. *J Geophys Res* 111:D06101. doi:10.1029/2005jd006061
- Garfinkel CI, Hartmann DL (2007) Effects of the El Niño–Southern oscillation and the quasi-biennial oscillation on polar temperatures in the stratosphere. *J Geophys Res* 112:D19112. doi:10.1029/2007jd008481
- Garfinkel CI, Hartmann DL (2008) Different ENSO teleconnections and their effects on the stratospheric polar vortex. *J Geophys Res* 113:D18114. doi:10.1029/2008jd009920
- Garfinkel CI, Hurwitz MM, Waugh DW, Butler AH (2012) Are the teleconnections of Central Pacific and Eastern Pacific El Niño distinct in boreal wintertime? *Clim Dyn* 41:1835–1852. doi:10.1007/s00382-012-1570-2
- Gent PR, Danabasoglu G, Donner LJ et al (2011) The community climate system model version 4. *J Clim* 24:4973–4991. doi:10.1175/2011jcli4083.1
- Hamilton K (1995) Interannual variability in the northern hemisphere winter middle atmosphere in control and perturbed experiments with the GFDL SKYHI general circulation model. *J Atmos Sci* 52:44–66. doi:10.1175/1520-0469(1995)052<0044:ivitnh>2.0.co;2
- Hegyí BM, Deng Y (2011) A dynamical fingerprint of tropical Pacific sea surface temperatures on the decadal-scale variability of cool-season Arctic precipitation. *J Geophys Res* 116:D20121. doi:10.1029/2011jd016001
- Hegyí BM, Deng Y, Black RX, Zhou RJ (2014) Initial transient response of the winter polar stratospheric vortex to idealized equatorial Pacific sea surface temperature anomalies in the NCAR WACCM. *J Clim* 27:2699–2713. doi:10.1175/jcli-d-13-00289.1
- Holland MM, Bailey DA, Briegleb BP, Light B, Hunke E (2012) Improved sea ice shortwave radiation physics in CCSM4: the impact of melt ponds and aerosols on arctic sea ice. *J Clim* 25:1413–1430. doi:10.1175/jcli-d-11-00078.1
- Hu Z-Z, Kumar A, Xue Y, Jha B (2014) Why were some La Niñas followed by another La Niña? *Clim Dyn* 42:1029–1042. doi:10.1007/s00382-013-1917-3
- Huang B, Hu Z-Z, Kinter JL, Wu Z, Kumar A (2012) Connection of stratospheric QBO with global atmospheric general circulation and tropical SST. Part I: methodology and composite life cycle. *Clim Dyn* 38:1–23. doi:10.1007/s00382-011-1250-7
- Ishii M, Shouji A, Sugimoto S, Matsumoto T (2005) Objective analyses of sea-surface temperature and marine meteorological variables for the 20th century using ICOADS and the KOBE collection. *Int J Climatol* 25:865–879. doi:10.1002/joc.1169
- Jackman CH, Marsh DR, Vitt FM, Garcia RR, Randall CE, Fleming EL, Frith SM (2009) Long-term middle atmospheric influence of very large solar proton events. *J Geophys Res* 114:D11304. doi:10.1029/2008jd011415
- Jiang N, Neelin JD, Ghil M (1995) Quasi-quadrennial and quasi-biennial variability in the equatorial Pacific. *Clim Dyn* 12(2):101–112. doi:10.1007/bf00223723
- Jin F-F, An S-I, Timmermann A, Zhao J (2003) Strong El Niño events and nonlinear dynamical heating. *Geophys Res Lett* 30:1120. doi:10.1029/2002gl016356
- Kalnay E, Kanamitsu M, Kistler R et al (1996) The NCEP/NCAR 40-year reanalysis project. *Bull Am Meteorol Soc* 77:437–471. doi:10.1175/1520-0477(1996)077<0437:tnyrp>2.0.co;2
- Kim KY, Kim YY (2002) Mechanism of Kelvin and Rossby waves during ENSO events. *Meteorol Atmos Phys* 81:169–189. doi:10.1007/s00703-002-0547-9
- Klein SA, Soden BJ, Lau NC (1999) Remote sea surface temperature variations during ENSO: evidence for a tropical atmospheric bridge. *J Clim* 12:917–932. doi:10.1175/1520-0442(1999)012<0917:rsstvd>2.0.co;2
- Kobayashi S, Ota Y, Harada Y, Ebita A et al (2015) The JRA-55 reanalysis: general specifications and basic characteristics. *J Meteorol Soc Jpn* 93:5–48. doi:10.2151/jmsj.2015-001
- Kumar A, Hoerling MP (2003) The nature and causes for the delayed atmospheric response to El Niño. *J Clim* 16:1391–1403. doi:10.1175/1520-0442-16.9.1391
- Labitzke K, van Loon H (1989) The Southern Oscillation. Part IX: the influence of volcanic eruptions on the Southern Oscillation in the stratosphere. *J Clim* 2:1223–1226. doi:10.1175/1520-0442(1989)002<1223:tsopit>2.0.co;2
- Lau NC, Leetmaa A, Nath MJ, Wang HL (2005) Influences of ENSO-induced Indo-Western Pacific SST anomalies on extratropical atmospheric variability during the boreal summer. *J Clim* 18:2922–2942. doi:10.1175/jcli3445.1
- Li Q, Ren RC, Cai M, Wu GX (2012) Attribution of the summer warming since 1970s in Indian Ocean Basin to the inter-decadal change in the seasonal timing of El Niño decay phase. *Geophys Res Lett* 39:L12702. doi:10.1029/2012gl052150
- Manzini E, Giorgetta MA, Esch M, Kornbluh L, Roeckner E (2006) The influence of sea surface temperatures on the northern winter stratosphere: ensemble simulations with the MAECHAM5 model. *J Clim* 19:3863–3881. doi:10.1175/jcli3826.1
- Marsh DR, Garcia RR, Kinnison DE, Boville BA, Sassi F, Solomon SC, Matthes K (2007) Modeling the whole atmosphere response to solar cycle changes in radiative and geomagnetic forcing. *J Geophys Res* 112:D23306. doi:10.1029/2006jd008306
- Marsh DR, Mills MJ, Kinnison DE, Lamarque J-F, Calvo N, Polvani LM (2013) Climate Change from 1850 to 2005 Simulated in CESM1(WACCM). *J Clim* 26:7372–7391. doi:10.1175/jcli-d-12-00558.1
- Matthes K, Marsh DR, Garcia RR, Kinnison DE, Sassi F, Walters S (2010) Role of the QBO in modulating the influence of the 11 year solar cycle on the atmosphere using constant forcings. *J Geophys Res* 115:D18110. doi:10.1029/2009jd013020

- Neale RB, Richter J, Park S, Lauritzen PH, Vavrus SJ, Rasch PJ, Zhang MH (2013) The mean climate of the Community Atmosphere Model (CAM4) in forced SST and fully coupled experiments. *J Clim* 26:5150–5168. doi:[10.1175/jcli-d-12-00236.1](https://doi.org/10.1175/jcli-d-12-00236.1)
- Newell RE, Weare BC (1976) Factors governing tropospheric mean temperature. *Science* 194:1413–1414. doi:[10.1126/science.194.4272.1413](https://doi.org/10.1126/science.194.4272.1413)
- Plumb RA (1985) On the three-dimensional propagation of stationary waves. *J Atmos Sci* 42(3):217–229
- Rao J, Ren RC (2016) A decomposition of ENSO's impacts on the northern winter stratosphere: competing effect of SST forcing in the tropical Indian Ocean. *Clim Dyn* 46:3689–3707. doi:[10.1007/s00382-015-2797-5](https://doi.org/10.1007/s00382-015-2797-5)
- Rao J, Ren RC, Yang Y (2014) Numerical simulations of the impacts of tropical convective heating on the intensity of the northern winter stratospheric polar vortex. *Chin J Atmos Sci* 38(6):1159–1171. doi:[10.3878/j.issn.1006-9895.1404.13268](https://doi.org/10.3878/j.issn.1006-9895.1404.13268) (in Chinese)
- Rao J, Ren RC, Yang Y (2015) Parallel comparison of the northern winter stratospheric circulation in reanalysis and in CMIP5 models. *Adv Atmos Sci* 32(7):952–966. doi:[10.1007/s00376-014-4192-2](https://doi.org/10.1007/s00376-014-4192-2)
- Rayner NA, Parker DE, Horton EB, Folland CK, Alexander LV, Rowell DP, Kent EC, Kaplan A (2003) Global analyses of sea surface temperature, sea ice, and night marine air temperature since the late nineteenth century. *J Geophys Res* 108:4407. doi:[10.1029/2002jd002670](https://doi.org/10.1029/2002jd002670)
- Reid G, Gage K, McAfee J (1989) The thermal response of the tropical atmosphere to variations in equatorial Pacific sea surface temperature. *J Geophys Res* 94:14705–14716. doi:[10.1029/jd094id12p14705](https://doi.org/10.1029/jd094id12p14705)
- Ren RC (2012a) Study of the lag-coupling between the timescale ENSO events and the stratospheric circulation in the past 60 years and its mechanism. *Acta Meteorol Sin* 70: 520–535. doi:[10.11676/qxxb2012.043](https://doi.org/10.11676/qxxb2012.043) (in Chinese)
- Ren RC (2012b) Seasonality of the lagged relationship between ENSO and the Northern Hemispheric polar vortex variability. *Atmos Ocean Sci Lett* 5:113–118. doi:[10.1080/16742834.2012.11446975](https://doi.org/10.1080/16742834.2012.11446975)
- Ren RC, Cai M, Xiang C, Wu G (2012) Observational evidence of the delayed response of stratospheric polar vortex variability to ENSO SST anomalies. *Clim Dyn* 38:1345–1358. doi:[10.1007/s00382-011-1137-7](https://doi.org/10.1007/s00382-011-1137-7)
- Richter JH, Sassi F, Garcia RR (2010) Toward a physically based gravity wave source parameterization in a general circulation model. *J Atmos Sci* 67(1):136–156. doi:[10.1175/2009jas3112.1](https://doi.org/10.1175/2009jas3112.1)
- Saravanan R, Chang P (2000) Interaction between tropical Atlantic variability and El Niño-Southern Oscillation. *J Clim* 13:2177–2194. doi:[10.1175/1520-0442\(2000\)013<2177:ibtava>2.0.co;2](https://doi.org/10.1175/1520-0442(2000)013<2177:ibtava>2.0.co;2)
- Sassi F, Kinnison D, Boville BA, Garcia RR, Roble R (2004) Effect of El Niño-Southern Oscillation on the dynamical, thermal, and chemical structure of the middle atmosphere. *J Geophys Res* 109:D17108. doi:[10.1029/2003jd004434](https://doi.org/10.1029/2003jd004434)
- Taguchi M, Hartmann DL (2006) Increased occurrence of stratospheric sudden warmings during El Niño as simulated by WACCM. *J Clim* 19:324–332. doi:[10.1175/jcli3655.1](https://doi.org/10.1175/jcli3655.1)
- Taylor KE, Stouffer RJ, Meehl GA (2012) An overview of CMIP5 and the experiment design. *Bull Am Meteorol Soc* 93:485–498. doi:[10.1175/bams-d-11-00094.1](https://doi.org/10.1175/bams-d-11-00094.1)
- Tozuka T, Yamagata T (2003) Annual ENSO. *J Phys Oceanogr* 33:1564–1578. doi:[10.1175/2414.1](https://doi.org/10.1175/2414.1)
- Uppala SM, Kallberg PW, Simmons AJ et al (2005) The ERA-40 re-analysis. *Q J R Meteorol Soc* 131:2961–3012. doi:[10.1256/qj.04.176](https://doi.org/10.1256/qj.04.176)
- van Loon H, Zerefos C, Repapis C (1982) The Southern Oscillation in the stratosphere. *Mon Weather Rev* 110:225–229. doi:[10.1175/1520-0493\(1982\)110<0225:tsoits>2.0.co;2](https://doi.org/10.1175/1520-0493(1982)110<0225:tsoits>2.0.co;2)
- Vimont DJ, Battisti DS, Hirst AC (2001) Footprinting: a seasonal connection between the tropics and mid-latitudes. *Geophys Res Lett* 28:3923–3926. doi:[10.1029/2001gl013435](https://doi.org/10.1029/2001gl013435)
- Wallace JM, Chang FC (1982) Interannual variability of the wintertime polar vortex in the Northern Hemisphere middle stratosphere. *J Meteorol Soc Jpn* 60:149–155
- Wang B, An SI (2005) A method for detecting season-dependent modes of climate variability: S-EOF analysis. *Geophys Res Lett* 32:L15710. doi:[10.1029/2005gl022709](https://doi.org/10.1029/2005gl022709)
- Wei K, Chen W, Huang R (2007) Association of tropical Pacific sea surface temperatures with the stratospheric Holton-Tan Oscillation in the Northern Hemisphere winter. *Geophys Res Lett* 34:L16814. doi:[10.1029/2007gl030478](https://doi.org/10.1029/2007gl030478)
- Xie F, Li J, Tian W, Feng J, Huo Y (2012) Signals of El Niño Modoki in the tropical tropopause layer and stratosphere. *Atmos Chem Phys* 12:5259–5273. doi:[10.5194/acp-12-5259-2012](https://doi.org/10.5194/acp-12-5259-2012)
- Yulaeva E, Wallace JM (1994) The signature of ENSO in global temperature and precipitation fields derived from the microwave sounding unit. *J Clim* 7:1719–1736. doi:[10.1175/1520-0442\(1994\)007<1719:tsoeig>2.0.co;2](https://doi.org/10.1175/1520-0442(1994)007<1719:tsoeig>2.0.co;2)